nature cell biology

A nuclear role for the respiratory enzyme CLK-1 in regulating mitochondrial stress responses and longevity

Richard M. Monaghan[1], Robert G. Barnes[1], Kate Fisher[1], Tereza Andreou[1,2], Nicholas Rooney[1,2], Gino B. Poulin[1,3] and Alan J. Whitmarsh[1,3]

The coordinated regulation of mitochondrial and nuclear activities is essential for cellular respiration and its disruption leads to mitochondrial dysfunction, a hallmark of ageing. Mitochondria communicate with nuclei through retrograde signalling pathways that modulate nuclear gene expression to maintain mitochondrial homeostasis. The monooxygenase CLK-1 (human homologue COQ7) was previously reported to be mitochondrial, with a role in respiration and longevity. We have uncovered a distinct nuclear form of CLK-1 that independently regulates lifespan. Nuclear CLK-1 mediates a retrograde signalling pathway that is conserved from *Caenorhabditis elegans* to humans and is responsive to mitochondrial reactive oxygen species, thus acting as a barometer of oxidative metabolism. We show that, through modulation of gene expression, the pathway regulates both mitochondrial reactive oxygen species metabolism and the mitochondrial unfolded protein response. Our results demonstrate that a respiratory enzyme acts in the nucleus to control mitochondrial stress responses and longevity.

Mitochondria function as cellular energy generators producing the fuel, predominantly in the form of adenosine triphosphate (ATP), required to drive biological processes. They act as a hub for many essential biochemical pathways, the metabolites of which are closely monitored by the cell[1–3]. Most of the enzymes that are required for these pathways are encoded by the nuclear genome compared with a few that are encoded directly by the mitochondrial genome. Therefore, coordinated regulation of nuclear and mitochondrial gene expression is essential[4,5]. Mitochondrial activity is monitored through a variety of mitochondrial readouts that include the amount of reactive oxygen species (ROS) produced during oxidative metabolism, the rate of ATP production, and the level of misfolded proteins. These readouts activate or inhibit cytosolic signalling pathways that ensure the appropriate changes in nuclear gene expression occur to maintain mitochondrial homeostasis[2–6].

Mitochondrial dysfunction is a hallmark of ageing and alterations in mitochondrial activity affect the lifespan of model organisms[7,8]. Indeed, increased mitochondrial ROS modulates stress responses and promotes longevity[3,8–10]. In addition, the initiation of a distinct mitochondrial to nuclear retrograde signalling pathway, the mitochondrial unfolded protein response (UPR^{mt}), has been proposed to extend lifespan[11–13]. These findings suggest a direct link between mitochondrial stress and longevity.

In *Caenorhabditis elegans*, mutants of components of the electron transport chain exhibit reduced oxidative phosphorylation and increased longevity[14]. The mitochondrial diiron-containing monooxygenase CLK-1 catalyses the hydroxylation of 5-demethoxyubiquinone, a critical step in the biosynthesis of ubiquinone, an essential cofactor of the electron transport chain[15,16]. However, *C. elegans clk-1* null mutants and heterozygous mice exhibit altered mitochondrial metabolism and extended lifespans through a pathway that seems to be independent of ubiquinone biosynthesis and ATP production[17–21]. This indicates that additional functions for CLK-1 may exist. CLK-1, and its human homologue COQ7, contain an amino-terminal mitochondrial targeting sequence (MTS) and are assumed to reside exclusively within mitochondria[22,23]. However, we have observed CLK-1 and COQ7 present in the nuclei of *C. elegans* and cultured human cells, respectively. Furthermore, we have uncovered a specific role for the nuclear pools of CLK-1 and COQ7 in the regulation of ROS metabolism, mitochondrial stress responses and longevity.

[1]Faculty of Life Sciences, University of Manchester, Michael Smith Building, Oxford Road, Manchester M13 9PT, UK. [2]Present addresses: Institute of Cancer and Pathology, University of Leeds, St James's University Hospital, Leeds LS9 7TF, UK (T.A.); The Beatson Institute for Cancer Research, Switchback Road, Bearsden, Glasgow G61 1BD, UK (N.R.).
[3]Correspondence should be addressed to G.B.P. or A.J.W. (e-mail: gino.poulin@manchester.ac.uk or alan.j.whitmarsh@manchester.ac.uk)

Received 11 December 2014; accepted 27 March 2015; published online 11 May 2015; DOI: 10.1038/ncb3170

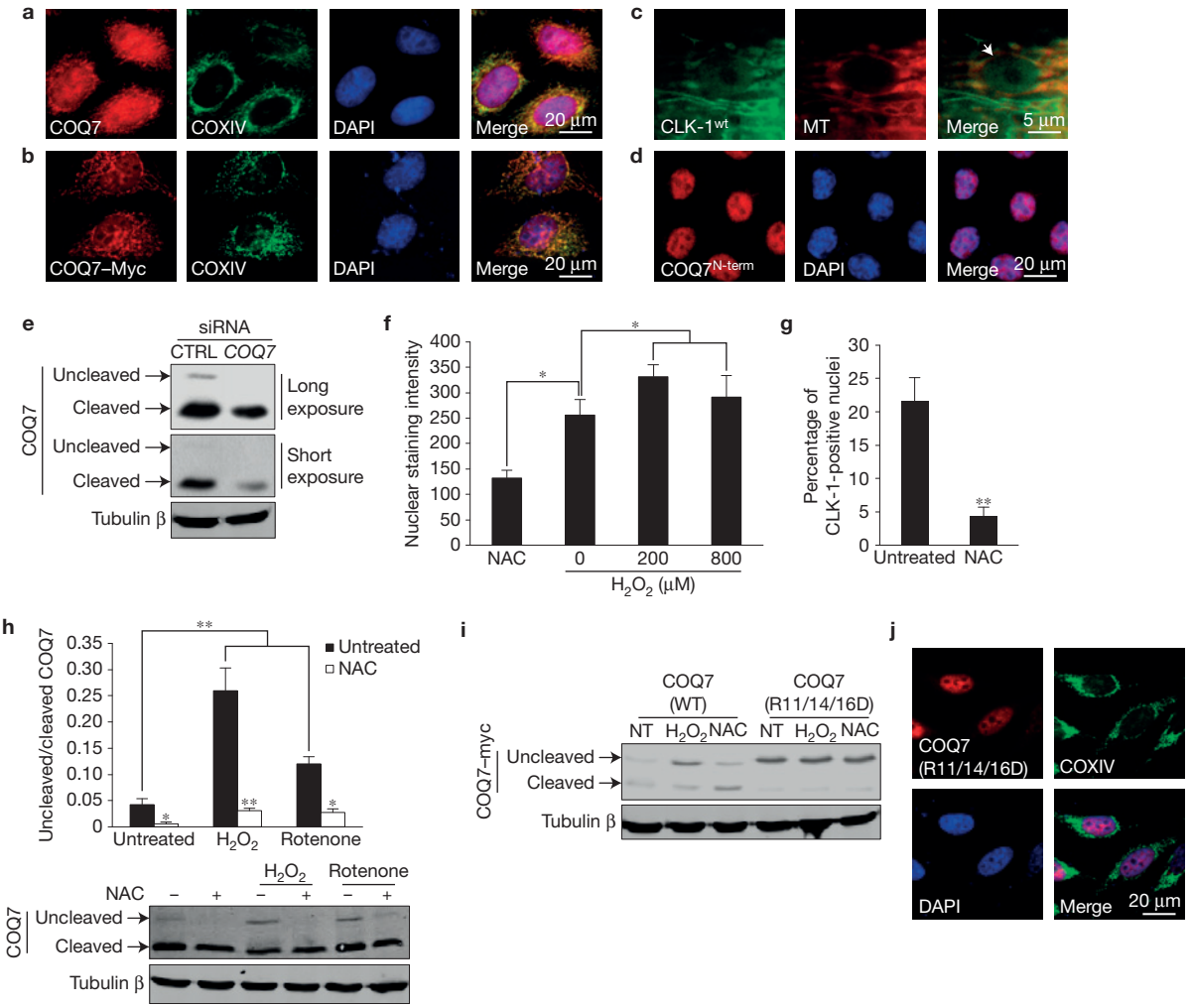

Figure 1 CLK-1 and its human homologue COQ7 localize to mitochondria and nuclei. (**a**) Endogenous COQ7 and COXIV (mitochondrial marker) immunostaining in HeLa cells. Nuclei were stained with DAPI. (**b**) HeLa cells expressing COQ7 tagged at the C terminus with a Myc epitope (COQ7–Myc) were stained with anti-Myc and anti-COXIV antibodies. Quantification of nuclear COQ7–Myc staining is shown in Supplementary Fig. 1a. (**c**) Wild-type CLK-1 (CLK-1^{wt}) fused at the C terminus to GFP localizes to both mitochondria and nuclei in adult *C. elegans*. The arrow marks a nucleus. MT (MitoTracker, mitochondrial marker). (**d**) HeLa cells immunostained with an antibody specific to the N terminus (amino acids 1–37) of COQ7 (COQ7$^{N\text{-}term}$). (**e**) siRNA targeting *COQ7* transcripts decreases the levels of both cleaved and uncleaved COQ7 protein. Immunoblots of lysates from HEK293 cells transfected with non-targeting (*CTRL*) or *COQ7* siRNA. Short and long exposures are shown. (**f**) Quantification of nuclear staining intensity of cells immunostained with anti-COQ7(1–37) (COQ7$^{N\text{-}term}$) following treatment with antioxidant (*N*-acetyl cysteine, NAC, 10 mM, 24 h) or exogenous ROS (hydrogen peroxide, 200 μM or 800 μM, respectively, 3 h) compared with untreated (0) control. Fifty cells were assessed per experiment in $n = 3$ independent experiments (error bars, s.e.m. $^{*}P < 0.05$). (**g**) Percentage of mCherry-positive nuclei that are also GFP-positive in *C. elegans* expressing CLK-1–GFP and the nuclear marker HIS-24–mCherry. Twenty-five worms were assessed per experiment in $n = 3$ independent experiments (error bars, s.e.m. $^{**}P < 0.005$). (**h**) The ratio of uncleaved to cleaved COQ7 in lysates from HEK293 was quantified from $n = 3$ independent immunoblotting experiments (error bars, s.e.m. $^{*}P < 0.05$, $^{**}P < 0.005$). Cells were treated with hydrogen peroxide (H_2O_2, 150 μM, 3 h; cellular ROS) or rotenone (50 μM, 3 h; complex I inhibitor, mitochondrial ROS), with or without 10 mM NAC. A representative immunoblot is shown. (**i**) Immunoblots of lysates from HEK293 cells expressing COQ7–Myc or COQ7 (R11/14/16D)–Myc (mutant that disrupts mitochondrial targeting) treated with H_2O_2 (150 μM, 4 h) or NAC (10 mM, 6 h). NT, untreated cells. (**j**) Blocking mitochondrial targeting of COQ7 enhances nuclear localization of uncleaved COQ7. HeLa cells expressing a C-terminally Myc-tagged COQ7 (R11/14/16D) mutant, which disrupts mitochondrial targeting, were immunostained with anti-Myc and anti-COXIV antibodies. Unprocessed original scans of immunoblots are shown in Supplementary Fig. 5.

RESULTS

CLK-1 and its human homologue COQ7 localize to mitochondria and nuclei

We found that endogenous and exogenously expressed COQ7 exhibit both mitochondrial and nuclear immunostaining in HeLa cells (Fig. 1a,b and Supplementary Fig. 1a). Consistent with this, adult transgenic worms expressing CLK-1 fused to green fluorescent protein (GFP) also exhibit fluorescence in both compartments (Fig. 1c). We identified a sequence in COQ7 between amino acids 11 and 29 that is required for nuclear localization (Supplementary Fig. 1b). This nuclear targeting sequence (NTS) is adjacent to the MTS, but within the N-terminal region that is cleaved and degraded by the mitochondrial processing peptidase (MPP) following mitochondrial import[23] (Fig. 2b). This suggested that a pool of COQ7, rather than being imported into

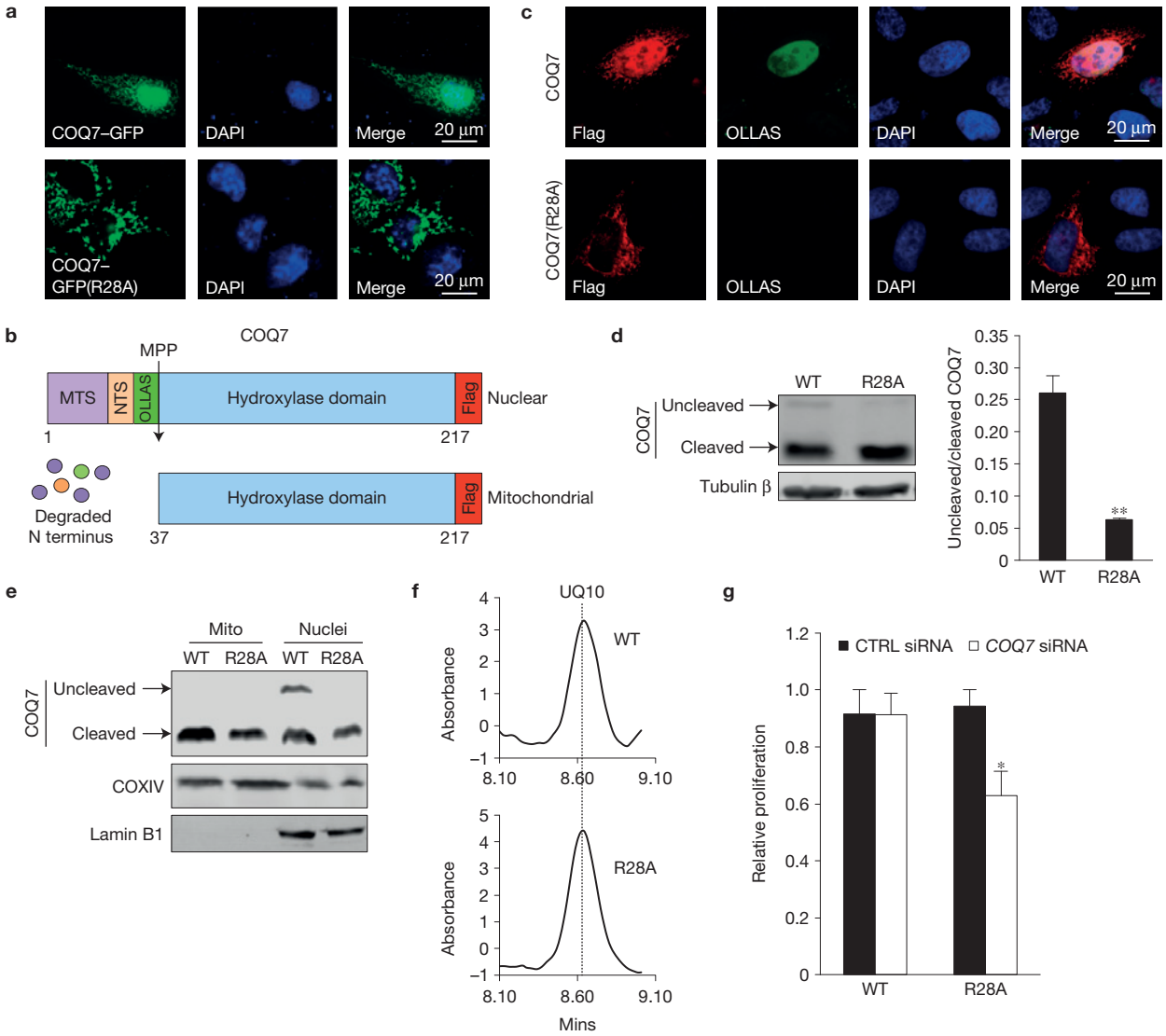

Figure 2 Nuclear COQ7 functions independently of the mitochondrial form. (**a**) Reduced nuclear localization of COQ7 (R28A) mutant. Fluorescence in COS7 cells expressing COQ7 or COQ7 (R28A) fused at the C terminus to GFP. Nuclei were stained with DAPI. (**b**) Schematic diagram depicting the location of the mitochondrial targeting sequence (MTS), the nuclear targeting sequence (NTS) and the mitochondrial processing peptidase cleavage site (MPP) on COQ7. The N-terminal region of COQ7 is degraded following cleavage by MPP in mitochondria. Also shown are the positions of the OLLAS and FLAG epitope tags. The numbers refer to amino-acid positions of COQ7. (**c**) HeLa cells expressing dual OLLAS- and FLAG-tagged COQ7 or COQ7 (R28A) immunostained with anti-FLAG and anti-OLLAS antibodies. The anti-FLAG antibodies recognize total COQ7 (uncleaved and cleaved) and the anti-OLLAS antibody specifically recognizes uncleaved nuclear COQ7. (**d**) Immunoblot of cell lysates from HEK293 cells stably expressing either untagged wild-type (WT) COQ7 or the R28A mutant in the presence of siRNA against untranslated regions of *COQ7*. Quantification of the ratio of uncleaved (nuclear) to cleaved (mitochondrial) COQ7 from $n=3$ independent experiments is presented (error bars, s.e.m. $^{**}P<0.005$). (**e**) Immunoblot of cell lysates from the stable HEK293 cells expressing either wild-type (WT) COQ7 or the R28A mutant separated into mitochondrial (Mito) and nuclear (Nuclei) pellet fractions (COXIV, mitochondrial marker; lamin B1, nuclear matrix marker). The presence of some COXIV and cleaved COQ7 in the nuclear fraction indicates that some mitochondrial contamination is present. (**f**) Ubiquinone (UQ10) levels are similar in COQ7 WT- and R28A-expressing cells. Reverse-phase HPLC chromatograms of quinones purified from cells (UQ10 peak at 8.63 min). (**g**) Proliferation of COQ7 (R28A)-expressing cells was reduced compared with COQ7 WT cells in the presence of siRNA targeting endogenous COQ7 (*COQ7* siRNA) but not control (CTRL) siRNA; measured by MTT assay (mean values from 4 wells of cells per condition in $n=3$ independent experiments; error bars, s.e.m. $^{*}P<0.05$). Cell survival was not altered under these conditions (see Supplementary Fig. 2f). Unprocessed original scans of immunoblots are shown in Supplementary Fig. 5.

mitochondria and cleaved, remains uncleaved and localizes to the nucleus. This scenario is supported by nuclear-specific immunostaining of endogenous COQ7 with antibodies that specifically recognize the N-terminal region (Fig. 1d and Supplementary Fig. 1c). It was also observed that two forms of COQ7 were visible on immunoblots of cell lysates and that both were decreased by *COQ7*-specific short interfering RNA (siRNA; Fig. 1e). These corresponded to the uncleaved and cleaved forms of the protein (Supplementary Fig. 1d). Taken together, these data establish that distinct mitochondrial and nuclear forms of COQ7 coexist within cells.

This dual localization of CLK-1 and COQ7 suggests that they may be part of a regulatory mechanism that links mitochondrial function

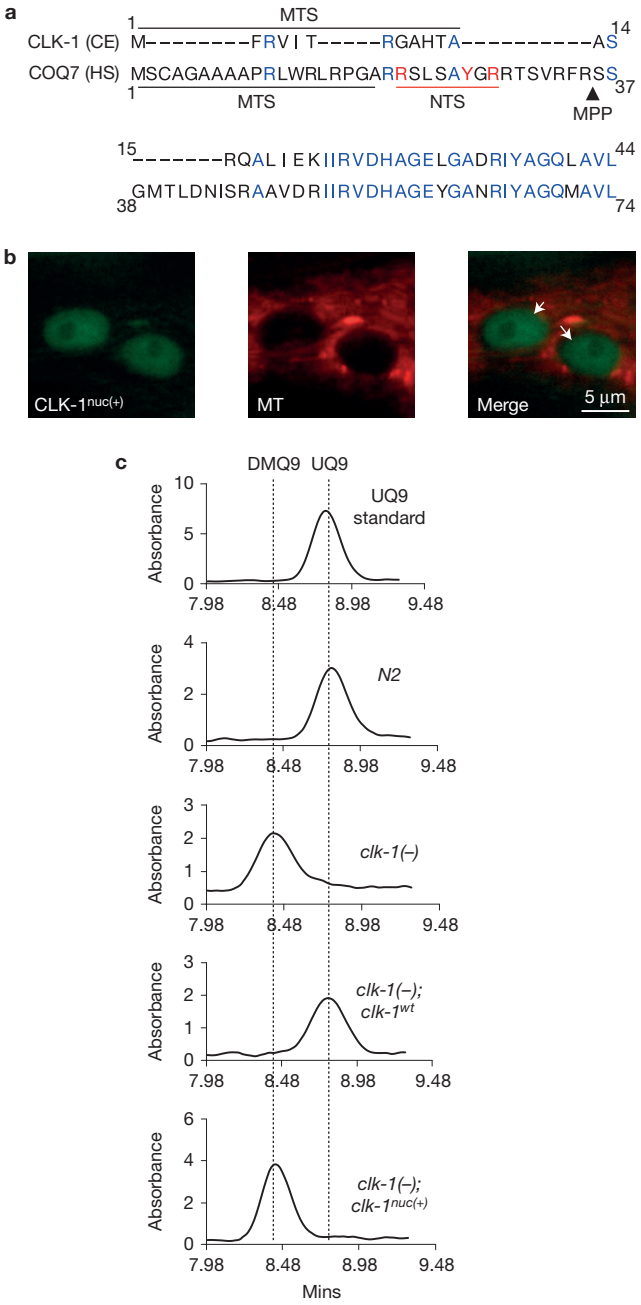

Figure 3 A truncated form of *C. elegans* CLK-1 with impaired mitochondrial targeting is predominantly nuclear and does not rescue ubiquinone biosynthesis. (**a**) The mechanism of targeting of *C. elegans* CLK-1 and human COQ7 to nuclei is not conserved. Alignment of the N termini and the start of the highly conserved diiron-binding domains of CLK-1 and COQ7. The mitochondrial targeting sequence (MTS) is denoted by the black bars, conserved amino acids are highlighted in blue, and the predicted mitochondrial processing peptidase (MPP) site in COQ7 is shown. The region in COQ7 containing determinants of nuclear localization (NTS) is denoted by the red bar and residues required for nuclear targeting are highlighted in red. CE, *C. elegans*; HS, *Homo sapiens*. The numbers refer to amino-acid positions. (**b**) CLK-1 lacking the MTS (CLK-$1^{nuc(+)}$) is predominantly nuclear in adult worms. Arrows mark nuclei. MT, MitoTracker (mitochondrial marker). (**c**) CLK-$1^{nuc(+)}$ expression does not rescue the loss of mitochondrial ubiquinone (UQ9) biosynthesis in *clk-1(–)* worms. Reverse-phase HPLC chromatograms of quinones extracted from the indicated strains (UQ9 peak at 8.78 min, DMQ9 peak at 8.42 min). CLK-1^{wt} but not CLK-$1^{nuc(+)}$ restores the UQ9 peak lost in *clk-1* (*clk-1(–)*) null worms.

to nuclear events. It has been proposed that the regulation of mitochondrial protein import in response to changes in ROS production and peptide efflux can act as a gauge of mitochondrial activity and dysfunction[11,24]. We found that the exposure of cells to an antioxidant (*N*-acetyl-L-cysteine; NAC) decreased the amount of nuclear COQ7 (Fig. 1f). The same treatment in worms reduced CLK-1–GFP nuclear localization (Fig. 1g). Conversely, an increase in ROS enhanced nuclear COQ7 levels (Fig. 1f) and this correlated with an increase in the amount of uncleaved COQ7 (Fig. 1h). To provide evidence that ROS regulation of mitochondrial import of COQ7 was a key determinant of its nuclear localization, we engineered a mutant with impaired mitochondrial targeting (COQ7 R11/14/16D). The mutant remained uncleaved and predominantly localized to nuclei, independently of ROS levels (Fig. 1i,j and Supplementary Fig. 1e). These data are consistent with a model in which a distinct pool of uncleaved COQ7 is targeted to the nucleus following inhibition of mitochondrial import through a ROS-dependent pathway.

Nuclear COQ7 functions independently of the mitochondrial form

To further characterize the nuclear targeting of COQ7, we performed site-directed mutagenesis of conserved residues within the N-terminal NTS (Supplementary Fig. 2a). We identified a point mutant (R28A) that, compared with wild-type COQ7, exhibited significantly reduced nuclear localization (Fig. 2a and Supplementary Fig. 2b). Furthermore, by inserting an epitope tag (OLLAS) immediately carboxy-terminal to the NTS but before the MPP cleavage site, we demonstrated that uncleaved wild-type COQ7 is present in nuclei but the R28A mutant is not (Fig. 2b,c). This is supported by immunoblots of cell lysates showing decreased amounts of uncleaved R28A mutant protein compared with the wild-type protein (Supplementary Fig. 2c). These data suggest that a pool of COQ7 can be redirected to the nucleus whereas the R28A mutant is predominantly targeted to mitochondria where it is cleaved.

As the loss of COQ7 expression would affect both its mitochondrial and nuclear functions, we created a system to specifically determine the effect of depleting nuclear COQ7. Cell lines were established with endogenous COQ7 expression replaced by ectopic expression of either wild-type COQ7 or the non-nuclear R28A mutant (Fig. 2d and Supplementary Fig. 2d). As expected, uncleaved wild-type COQ7 resided in the nuclear fraction but the uncleaved form was absent in the R28A-expressing cells (Fig. 2e). Importantly, both cell lines had normal levels of ubiquinone (Fig. 2f and Supplementary Fig. 2e). The loss of nuclear COQ7 resulted in a decreased cell count that, in the absence of an increase in cell death, was indicative of impaired proliferation (Fig. 2g and Supplementary Fig. 2f). These data demonstrate that COQ7 has a biologically relevant nuclear role that is independent of its characterized mitochondrial function in ubiquinone biosynthesis.

A truncated form of *C. elegans* CLK-1 with impaired mitochondrial targeting is predominantly nuclear and does not rescue ubiquinone biosynthesis

The N termini of *C. elegans* CLK-1 and human COQ7 are not well conserved compared with the high conservation of their diiron-binding domains that are C-terminal to their predicted MPP cleavage sites (Fig. 3a). Indeed, the N-terminal residues we identified as being

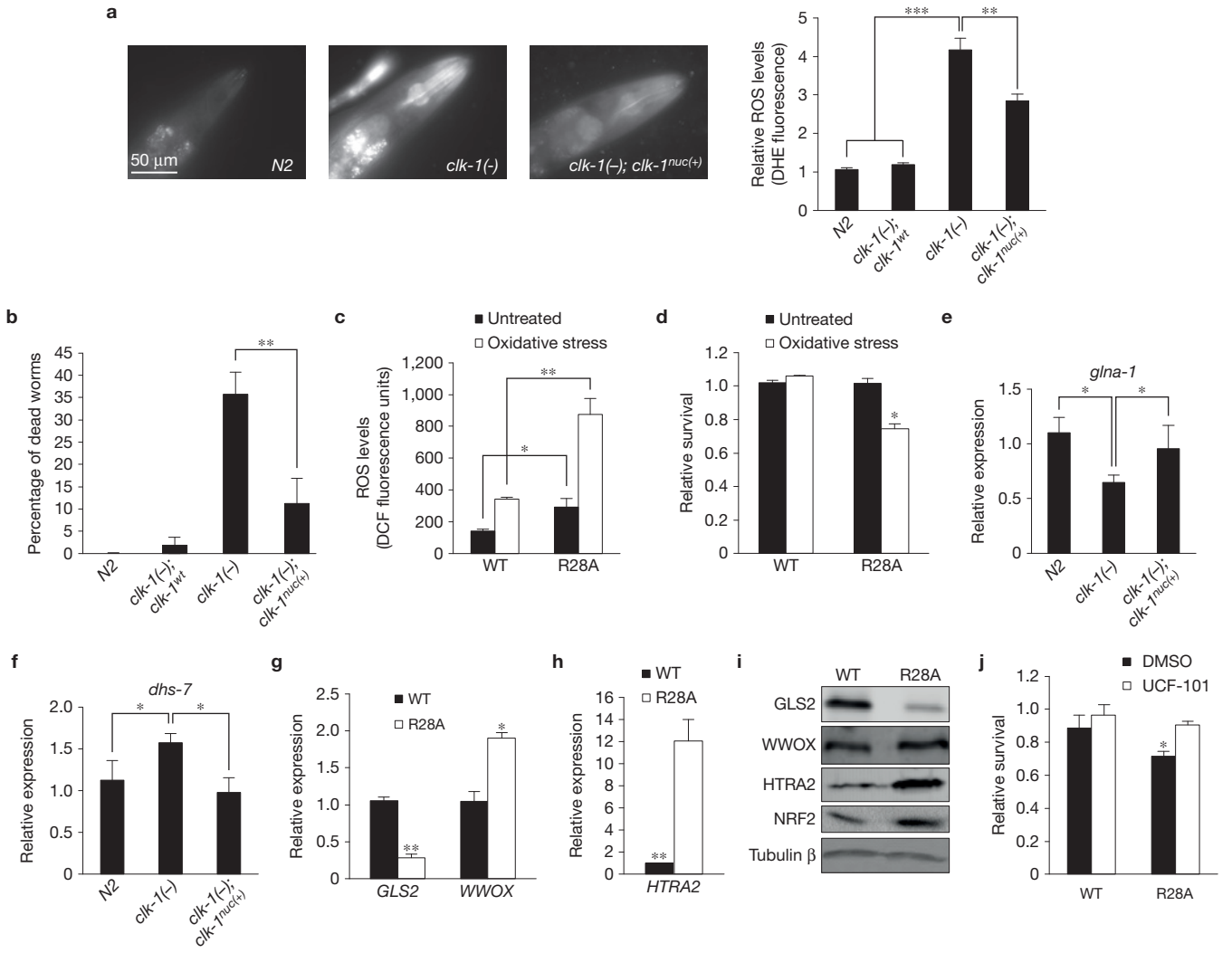

Figure 4 Nuclear CLK-1 and COQ7 regulate ROS metabolism. (**a**) Nuclear CLK-1 acts to lower cellular ROS levels. Expression of the nuclear form of CLK-1 (*clk-1*$^{nuc(+)}$) in *clk-1* null worms (*clk-1(–)*) partially rescues the increased levels of ROS observed in these worms measured using the ROS-sensitive dye DHE. Wild-type CLK-1–GFP (*clk-1*^{wt}) completely rescues the phenotype. Representative images and quantification of ROS levels are shown (25 worms assessed per experiment in $n=3$ independent experiments; error bars, s.e.m. $^{**}P<0.005$, $^{***}P<0.001$). (**b**) Expression of CLK-1$^{nuc(+)}$ in *clk-1* null worms significantly increases their survival in response to treatment with the respiratory inhibitor Paraquat (40 mM, 6 h). CLK-1^{wt} expression in *clk-1* null worms rescues survival to levels similar to *N2* worms (25 worms assessed per experiment in $n=3$ independent experiments; error bars, s.e.m. $^{**}P<0.01$). (**c**) Increased levels of ROS in untreated and oxidative-stress-treated (100 µM *tert*-butyl hydroperoxide, 1 h) HEK293 cells transfected with *COQ7* siRNA and expressing non-nuclear COQ7 (R28A) compared with wild type (WT), monitored by DCF fluorescence (mean values from 4 wells of cells per condition in $n=3$ independent experiments; error bars, s.e.m. $^{*}P<0.05$, $^{**}P<0.005$). (**d**) Nuclear COQ7 promotes resistance to ROS insult. Increased sensitivity of R28A-expressing cells to oxidative stress (1 mM $CoCl_2$, 4 h) measured by MTT assay (mean values from 4 wells of cells per condition in $n=3$ independent experiments; error bars, s.e.m. $^{*}P<0.05$). (**e**,**f**) Nuclear CLK-1 regulates the expression of genes involved in ROS metabolism. Altered transcript levels of *glna-1* and *dhs-7* in *clk-1* null worms (*clk-1(–)*) are rescued by expression of CLK-1$^{nuc(+)}$ (mean values from 3 reactions per condition for $n=3$ independent experiments; error bars, s.e.m. $^{*}P<0.05$). (**g**) The transcript levels of *GLS2* and *WWOX* are decreased or increased, respectively, on loss of nuclear COQ7 (R28A compared with WT; mean values from 3 reactions per condition for $n=4$ independent experiments; error bars, s.e.m. $^{*}P<0.05$, $^{**}P<0.005$). (**h**) The transcript levels of *HTRA2* are increased in cells lacking nuclear COQ7 (R28A compared with WT; mean values from 3 reactions per condition for $n=4$ independent experiments; error bars, s.e.m. $^{**}P<0.005$). (**i**) Immunoblots of corresponding protein levels for gene transcripts analysed in **g**,**h** and Supplementary Fig. 3c (NRF2). Unprocessed original scans of blots are shown in Supplementary Fig. 5. (**j**) Inhibition of HTRA2 activity (10 mM UCF-101, 30 min) rescues the ROS sensitivity of COQ7 (R28A) cells following oxidative stress (1 mM $CoCl_2$, 4 h). Cell survival measured by MTT assay relative to dimethylsulphoxide (DMSO)-treated cells (mean values from 4 wells of cells per condition in $n=3$ independent experiments; error bars, s.e.m. $^{*}P<0.05$).

critical for nuclear localization of COQ7 do not seem to be conserved in CLK-1. However, both homologues localize to the nucleus in a ROS-dependent manner (Fig. 1). This suggests that, although their nuclear role may be conserved, the precise molecular mechanism by which they are targeted to nuclei may be distinct. To address the non-mitochondrial function of worm CLK-1, we generated a transgenic animal featuring a single copy insertion expressing CLK-1 with the predicted 13-residue MTS deleted and GFP fused at its C terminus.

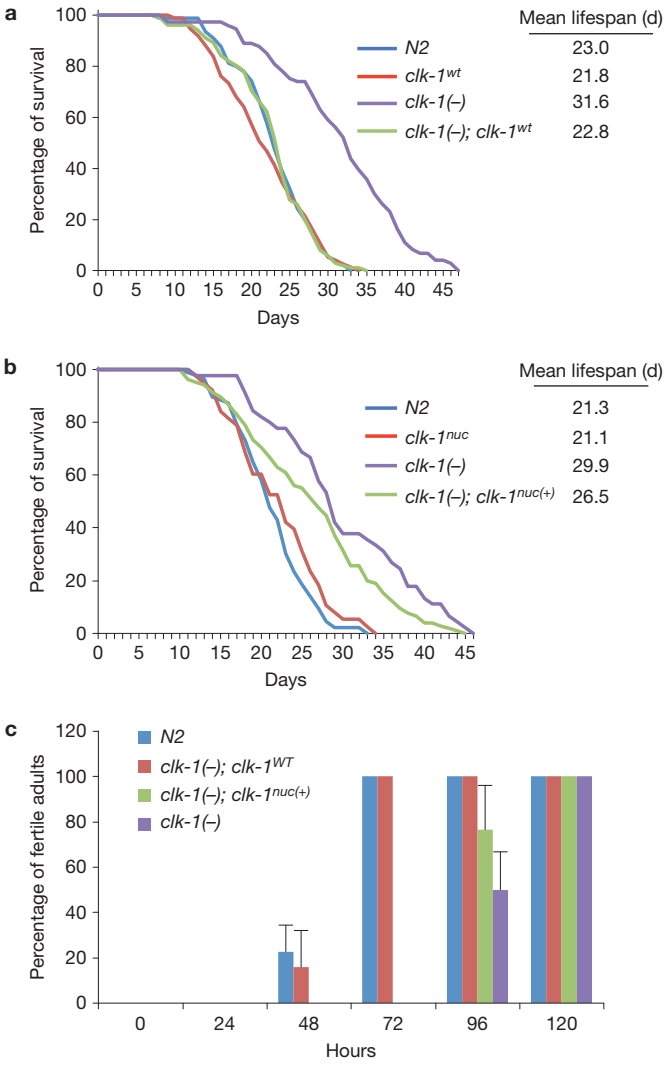

Figure 5 Mitochondrial and nuclear CLK-1 independently contribute to longevity. (**a**,**b**) CLK-1$^{nuc(+)}$ expression partially rescues the increased lifespan observed in *clk-1*(−) worms whereas CLK-1^{wt} completely rescues the longevity phenotype. The graphs show lifespan plotted as a percentage of survival and the mean lifespans calculated. *N2* is the wild-type strain. Lifespan data, including mean, maximum and 90th percentile lifespan with statistical analysis, for $n=3$ independent experiments are reported in Supplementary Table 1. (**c**) Analysis of developmental timing. Worms were synchronized at L1 and larval stage was determined every 24 h until all of the worms reached adulthood. Approximately 50 worms per genotype were monitored for each time point (mean values from $n=3$ independent experiments; error bars, s.e.m.).

This protein localized predominantly to the nucleus, demonstrating that, similar to COQ7, when mitochondrial targeting is impaired, nuclear localization is prevalent (Fig. 3b). We next crossed transgenic worms expressing either full-length CLK-1 (*clk-1*^{wt}) or this truncated nuclear-only form of CLK-1 (*clk-1*$^{nuc(+)}$) with the *clk-1* null worm *qm30* (*clk-1(−)*). As expected, full-length CLK-1 was able to rescue ubiquinone biosynthesis in these worms; however, CLK-1$^{nuc(+)}$ could not (Fig. 3c). This infers that, similar to nuclear COQ7 in human cells, nuclear CLK-1 does not contribute to the mitochondrial biosynthetic role of CLK-1 in worms.

Nuclear CLK-1 and COQ7 regulate ROS metabolism

It has been reported that *clk-1* null worms have increased mitochondrial ROS and are more sensitive to high levels of oxidative stress[25,26]. We therefore analysed the role of nuclear CLK-1 in modulating ROS responses. Expression of CLK-1$^{nuc(+)}$ in *clk-1* null worms partially rescued the increased ROS levels observed in these animals (Fig. 4a). CLK-1$^{nuc(+)}$ was also able to significantly rescue the ROS-sensitivity phenotype of *clk-1* null worms when exposed to the mitochondrial respiratory chain inhibitor Paraquat (Fig. 4b). Importantly, in human cells lacking nuclear COQ7, we also observed increased basal and induced levels of ROS (Fig. 4c) and these cells exhibited increased sensitivity to ROS-induced cell death (Fig. 4d). These results indicate that there is a conserved role for nuclear CLK-1 in the response of cells to ROS, potentially through regulation of ROS metabolism.

Mitochondrial glutamine metabolism is a key regulator of cellular redox balance and its inhibition is linked to increased ROS levels in cancer cells[27,28]. We examined whether the expression of the mitochondrial form of glutaminase (GLNA-1 in worms/GLS2 in humans), which converts glutamine to glutamate, was regulated in a nuclear CLK-1-dependent manner. In *clk-1* null worms, *glna-1* transcript levels were decreased compared with wild-type animals, an effect that was rescued in the presence of CLK-1$^{nuc(+)}$ (Fig. 4e and Supplementary Fig. 3a). Loss of nuclear COQ7 in human cells also resulted in a decrease in the expression of the *glna-1* homologue *GLS2* (Fig. 4g,i and Supplementary Fig. 3d). These data suggest that nuclear CLK-1 and COQ7 may regulate cellular ROS levels by promoting glutamine metabolism. Another regulator of ROS metabolism is the oxidoreductase WWOX, a hyperactivated form of which has been shown to increase cellular ROS levels in *Drosophila melanogaster*[29]. Interestingly, the transcript levels of one of the worm *WWOX* homologues are increased in *clk-1* null worms[30]. We found that expression of CLK-1$^{nuc(+)}$ could rescue the increased expression of the closest *WWOX* homologue, *dhs-7*, in *clk-1* null worms, and that human *WWOX* expression was increased on loss of nuclear COQ7 (Fig. 4f,g,i and Supplementary Fig. 3a,d). Taken together, these data suggest that nuclear CLK-1 and COQ7 can potentially regulate metabolic pathways that alter cellular ROS production independently of ubiquinone.

As cellular ROS levels were changed in a nuclear CLK-1-dependent manner, we sought to determine whether ROS-dependent gene expression was also altered. We found that transcripts of *sod-2*, encoding a ROS detoxification enzyme, were increased in *clk-1* null worms as previously reported[26]. Furthermore, transcripts of *skn-1*, encoding a transcription factor that is a central regulator of ROS homeostatic gene expression[31], were also increased (Supplementary Fig. 3b). The expression of nuclear CLK-1 in *clk-1* null worms abrogated the increased transcript levels of these genes (Supplementary Fig. 3b). Human homologues of *sod-2* and *skn-1*, *SOD2* and *NRF2* respectively, and the NRF2 target gene *HMOX1* were also increased in cells lacking nuclear COQ7 (Fig. 4i and Supplementary Fig. 3c). Our data indicate that the increased ROS levels observed in the absence of nuclear CLK-1 or COQ7 promote a ROS-defensive gene expression program. However, as the loss of nuclear CLK-1 or COQ7 sensitizes cells to oxidative stress (Fig. 4b,d) even in the presence of these increased ROS defences, it suggests that survival pathways may also be altered. To address this, we

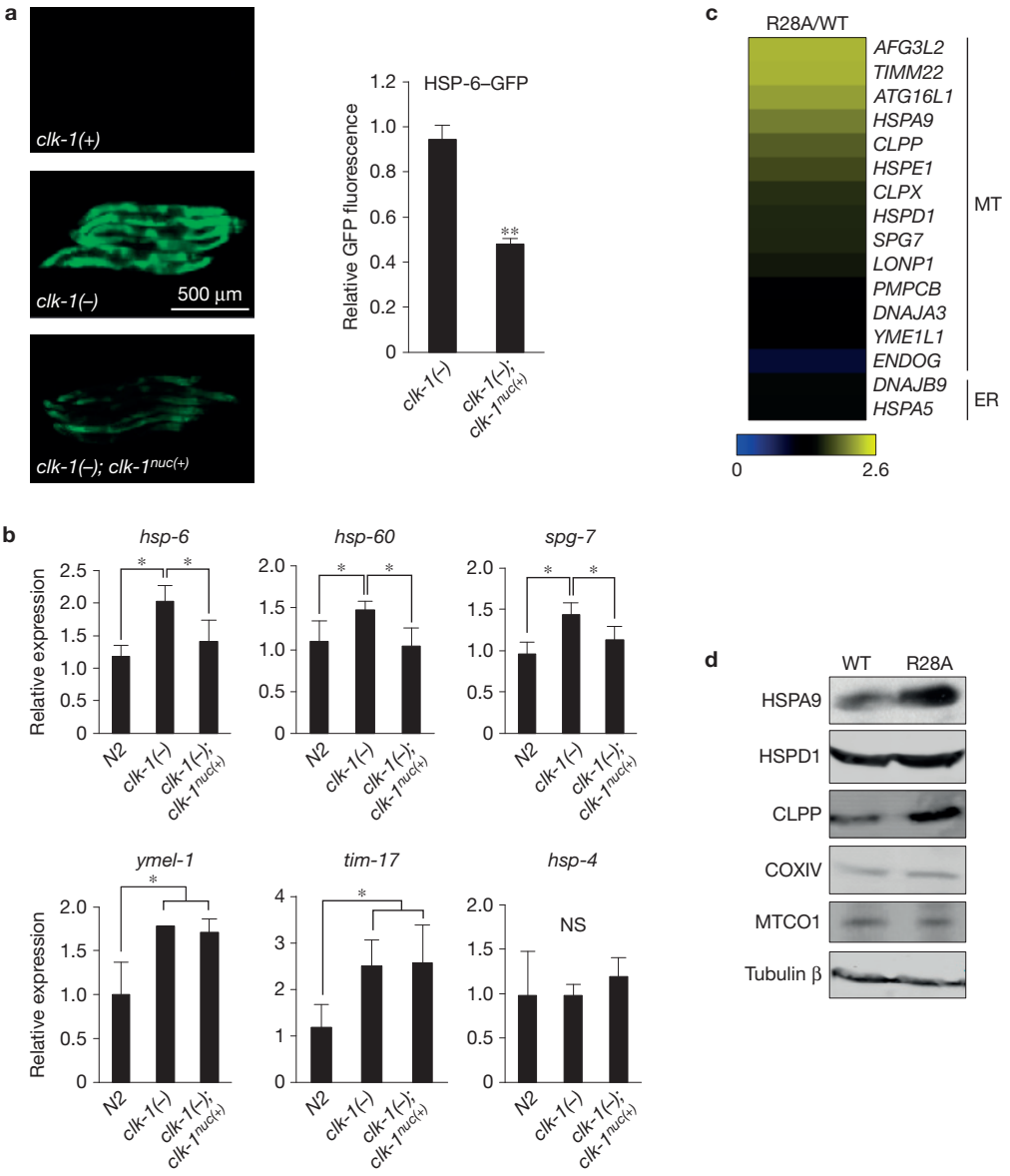

Figure 6 Nuclear CLK-1 and COQ7 suppress the expression of a subset of UPR^{mt} genes. (**a**) CLK-1$^{nuc(+)}$-expressing worms exhibit decreased *hsp-6::gfp* reporter activity compared with *clk-1(−)* worms. The unmodified *hsp-6::gfp* reporter strain is designated *clk-1*(+). Quantification of reporter fluorescence in CLK-1$^{nuc(+)}$-expressing worms (*clk-1(−); clk-1$^{nuc(+)}$*) relative to *clk-1(−)* worms (mean fluorescence of 50 worms per genotype pooled from $n=3$ independent experiments; error bars, s.e.m. $^{**}P<0.005$). (**b**) qPCR measuring mRNA transcripts of UPR^{mt} genes in *clk-1(−)* or *clk-1(−); clk-1$^{nuc(+)}$* worms relative to the wild-type strain (*N2*; mean values from 3 reactions per condition in $n=3$ independent experiments; error bars, s.e.m., NS, no significant difference, $^{*}P<0.05$). (**c**) Heat map depicting change in expression of UPR^{mt} genes (MT) and UPR^{ER} (ER) genes in R28A cells compared with WT COQ7 cells. The map is generated from the qPCR data presented in Supplementary Fig. 4b and is representative of $n=3$ independent experiments. Scale represents mean fold change in expression. (**d**) Immunoblots of levels of UPR^{mt} proteins including the mitochondrial controls COXIV (nuclear-encoded) and MTCO1 (mitochondrial-encoded). Unprocessed original scans of immunoblots are shown in Supplementary Fig. 5.

examined the expression of the pro-apoptotic mitochondrial protease HTRA2, which is stimulated through a ROS-dependent retrograde pathway activated by disruption to mitochondrial proteostasis[32]. HTRA2 levels were significantly increased in cells lacking nuclear COQ7 (Fig. 4h,i and Supplementary Fig. 3d) and the inhibition of HTRA2 activity rescued the ROS-sensitivity phenotype of these cells (Fig. 4j). These data support a role for nuclear CLK-1 and COQ7 in regulating retrograde ROS responses through modulation of gene expression.

Mitochondrial and nuclear CLK-1 independently contribute to longevity

In addition to changes in ROS metabolism, *C. elegans clk-1* null mutants and heterozygous mice have extended lifespans[17,21]. *C. elegans* lacking CLK-1 survive by obtaining ubiquinone from their diet and heterozygous mice exhibit wild-type ubiquinone levels, suggesting that their increased longevity may be unrelated to the function of CLK-1 in ubiquinone biosynthesis[19,21]. Interestingly, the expression of CLK-1$^{nuc(+)}$ in *clk-1* null worms caused a decrease in their enhanced

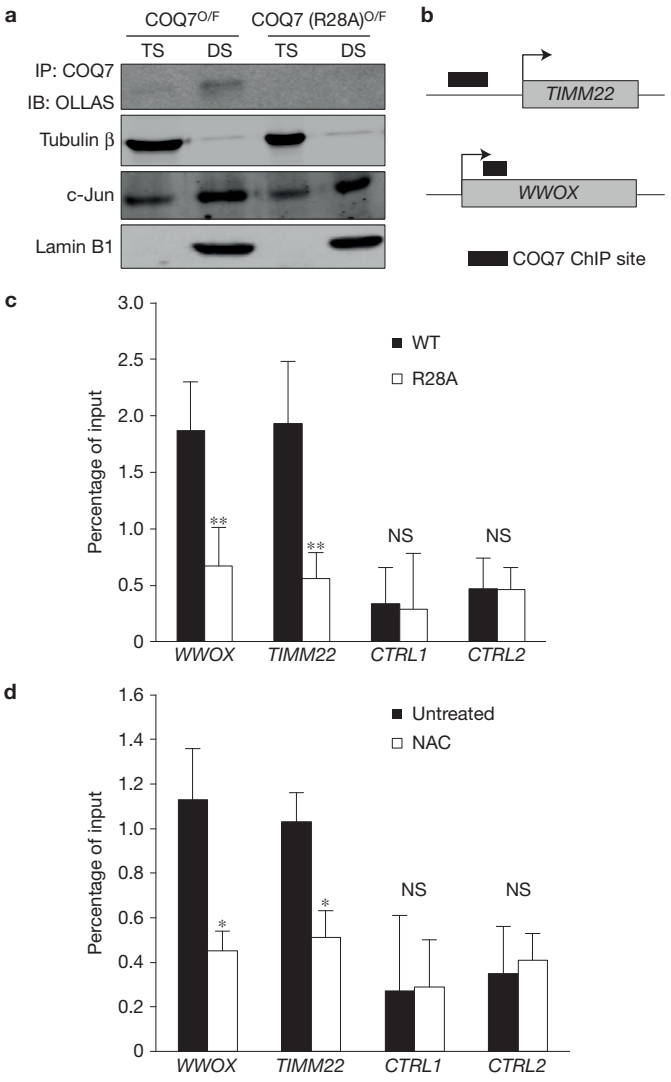

Figure 7 COQ7 associates with chromatin. (**a**) Chromatin fractionation of HEK293 cells expressing wild-type or R28A (non-nuclear mutant) COQ7 tagged with an internal OLLAS epitope (as shown in Fig. 2b) followed by anti-COQ7 immunoprecipitation and anti-OLLAS immunoblotting. Each fraction was also immunoblotted for the markers tubulin β (cytosolic), c-Jun (active chromatin) and lamin B1 (nuclear matrix). TS, Triton-soluble fraction; DS, DNase-soluble fraction. (**b**) Schematic of the *WWOX* and *TIMM22* COQ7-associated promoter sites enriched in anti-COQ7 ChIPs compared with the IgG control. Arrows denote transcriptional start sites. Full data set of enriched sites are provided in Supplementary Table 2. (**c**) Anti-COQ7 ChIP was performed on HEK293 cells expressing wild-type (WT) or the non-nuclear form (R28A) of COQ7 before qPCR analysis of *WWOX* and *TIMM22* promoter sites and two control intergenic sites (*CTRL1* and *CTRL2*; mean values from 3 reactions per condition in $n=3$ independent experiments; error bars, s.e.m. NS, no significant difference; $^{**}P<0.005$). (**d**) Anti-COQ7 ChIP was performed on HEK293 cells treated with antioxidant (*N*-acetyl cysteine, NAC, 10 mM, 24 h) compared with untreated (mean values from 3 reactions per condition in $n=3$ independent experiments; error bars, s.e.m. NS, no significant difference; $^{*}P<0.05$). Unprocessed original scans of immunoblots are shown in Supplementary Fig. 5.

longevity phenotype (Fig. 5a,b and Supplementary Table 1). This infers that nuclear CLK-1 can regulate longevity and that this is unrelated to the mitochondrial role of CLK-1 in ubiquinone biosynthesis. It also suggests that nuclear and mitochondrial CLK-1 regulate lifespan through distinct mechanisms. The expression of CLK-1$^{nuc(+)}$ did not rescue the delayed larval development observed in *clk-1* null worms[17] (Fig. 5c), which is consistent with this phenotype being due to the loss of mitochondrial CLK-1.

Nuclear CLK-1 and COQ7 suppress the expression of a subset of UPR^{mt} genes

The extended lifespans of *clk-1* mutants, and other mitochondrial longevity phenotypes, have been linked to activation of a distinct mitochondrial to nuclear retrograde pathway, the mitochondrial unfolded protein response[11,12] (UPR^{mt}). The UPR^{mt} responds to mitochondrial dysfunction by regulating nuclear gene expression[13] and there is an increase in the expression of some UPR^{mt}-responsive genes in *clk-1* null worms[11,30]. Thus, it is plausible that there could be crosstalk between CLK-1 nuclear signalling and the UPR^{mt}. Indeed, we found that the expression of an UPR^{mt}-responsive fluorescent reporter, which is activated in *clk-1* null worms, was significantly reduced in the presence of CLK-1$^{nuc(+)}$ (Fig. 6a). This indicates that nuclear CLK-1 may potentially act as a suppressor of the UPR^{mt}. We subsequently monitored transcript levels for a range of UPR^{mt} genes[11,33] and identified a subset (*hsp-6*, *hsp-60*, *spg-7*) where increased expression in *clk-1* null worms was abrogated by expression of CLK-1$^{nuc(+)}$ (Fig. 6b and Supplementary Fig. 4a). Importantly, this regulation of the UPR^{mt} was conserved as the suppressed expression of homologues of these genes (*HSPA9*, *HSPD1*, *AFG3L2*) and of other UPR^{mt}-associated genes (*ATG16L1*, *CLPP*, *CLPX*, *HSPE1*, *LONP1*, *SPG7*, *TIMM22*) was relieved on loss of nuclear COQ7 in human cells (Fig. 6c,d and Supplementary Fig. 4b). The UPR^{mt} can be activated by an imbalance between mitochondrial- and nuclear-encoded mitochondrial proteins[12] but this was not observed in cells lacking nuclear COQ7 (Fig. 6d and Supplementary Fig. 4c; compare MTCO1 to COXIV). Furthermore, we noted that some of the UPR^{mt}-associated genes that were not regulated by nuclear COQ7 (*DNAJA3*, *ENDOG*, *PMPCB*, *tim-17*, *ymel-1/YME1L1*) are downstream targets of a distinct UPR^{mt} instigated in the mitochondrial matrix[33] (Fig. 6b,c and Supplementary Fig. 4a,b). These data, therefore, demonstrate that nuclear CLK-1 and COQ7 can selectively suppress a branch of the UPR^{mt}.

COQ7 associates with chromatin

As we have demonstrated that nuclear CLK-1 and COQ7 have a role in regulating gene expression, we investigated a possible direct association with chromatin and components of the gene expression machinery. We performed chromatin fractionation of cells expressing COQ7 or the non-nuclear R28A mutant and found that the uncleaved form of COQ7, but not the R28A mutant, was enriched in the chromatin fraction (Fig. 7a). This suggests that nuclear COQ7 can associate directly with DNA–protein complexes. We next performed chromatin immunoprecipitation (ChIP) for endogenous COQ7 followed by promoter microarray (ChIP-on-chip) analysis. We uncovered a number of unique promoter sites enriched in COQ7 ChIPs compared with the IgG control (Supplementary Table 2). Interestingly, we identified *WWOX* and *TIMM22* as genes with sites enriched in the COQ7 ChIP (Fig. 7b) and whose expression is potentially regulated by nuclear COQ7 (Figs 4g and 6c). To provide additional confirmation that these were COQ7 chromatin-binding sites, we performed ChIP followed by qPCR targeting these

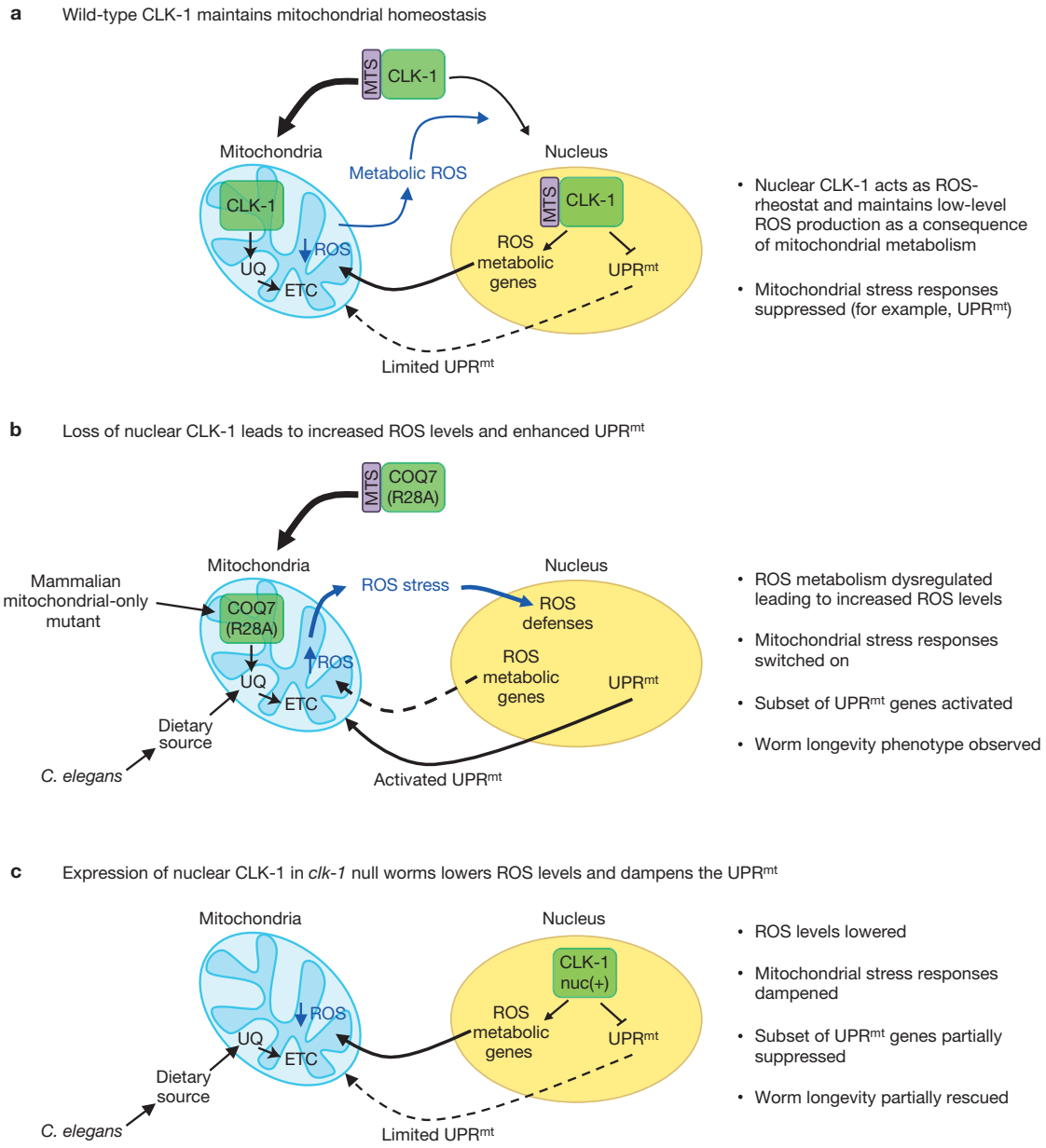

Figure 8 Model for the regulation of ROS metabolism, the UPR^{mt} and lifespan by nuclear CLK-1. (**a**) CLK-1 regulates mitochondrial homeostasis. Most CLK-1 localizes to mitochondria by means of its mitochondrial targeting sequence (MTS), where it is required for the biosynthesis of ubiquinone (UQ), an essential cofactor in the electron transport chain (ETC). However, basal levels of ROS, produced by the mitochondria, direct a pool of CLK-1 to the nucleus where it regulates gene expression. Some CLK-1-regulated genes are directly involved in mitochondrial ROS metabolism and, therefore, the prolonged presence of CLK-1 in the nucleus lowers ROS levels. Reduced ROS leads to CLK-1 being predominantly localized to mitochondria, and not the nucleus, so its affects on gene expression are relieved, basal ROS production returns, and homeostasis is maintained. (**b**) Loss of nuclear COQ7 (R28A mutant) in human cells or loss of CLK-1 in worms (that scavenge UQ from their bacterial diet) alters ROS metabolism leading to increased ROS levels, augments the UPR^{mt}, and extends the lifespan of worms. (**c**) The increased ROS levels, augmented UPR^{mt} and extended lifespan in *clk-1(−)* worms were suppressed by expression of a nuclear-localized CLK-1 mutant (CLK-1$^{nuc(+)}$) that acts to try to maintain mitochondrial homeostasis.

sites. Cells expressing wild-type COQ7 exhibited an enhanced ChIP signal compared with those expressing the non-nuclear R28A mutant (Fig. 7c). Furthermore, the ChIP signals for endogenous COQ7 at the *WWOX* and *TIMM22* sites were decreased following treatment with the antioxidant NAC (Fig. 7d), which would correlate with the decrease in the amount of nuclear COQ7 observed under such conditions (Fig. 1f). These data establish that the nuclear pool of COQ7 can directly associate with chromatin and that this may contribute to its ability to regulate gene expression.

DISCUSSION

We have uncovered a conserved role for the respiratory enzyme CLK-1 as a direct mediator of mitochondrial to nuclear retrograde signalling that responds to changes in cellular oxidative status and regulates

mitochondrial ROS metabolism, proteostasis and longevity (Fig. 8). CLK-1 was previously assumed to modulate lifespan solely by acting in mitochondria. Indeed, *clk-1* null worms have defective oxidative phosphorylation[34] and, similar to the many other respiration mutants that are long-lived[14], this is likely to contribute to their increased lifespan. We have now established that a nuclear form of CLK-1 acts independently to limit longevity, suggesting that the mitochondrial and nuclear forms of the protein contribute to lifespan phenotypes through distinct mechanisms.

Our data suggest that the nuclear role of CLK-1 and COQ7 may be to regulate gene expression; however, the exact mechanism is unclear. COQ7 associates with a significant number of genomic loci but how it promotes or suppresses transcription remains to be elucidated. It will be important to determine whether the enzymatic activity of COQ7 plays a role or whether it is involved in the recruitment of other transcriptional regulators. There is precedent for mitochondrial enzymes associating with nuclear genes; the yeast enzyme Arg5,6 participates in arginine biosynthesis but also binds to nuclear targets and modulates transcription[35].

The elevation of ROS signalling and activation of the UPR^{mt} are reported to promote longevity[10,12,25,36,37]; thus, the modulation of these pathways by nuclear CLK-1 would be consistent with its role in limiting lifespan. Our data suggest that nuclear CLK-1 and COQ7 function as a rheostat to maintain ROS homeostasis and dampen stress-responsive pathways such as the UPR^{mt}. In such a model, basal levels of ROS, produced by mitochondria during normal functioning, direct a pool of CLK-1 to the nucleus where it regulates gene expression. Some CLK-1-regulated genes are directly involved in mitochondrial ROS metabolism and, therefore, the prolonged presence of CLK-1 in the nucleus could instigate a decrease in ROS production. Reduced ROS leads to CLK-1 being predominantly localized to mitochondria, and not the nucleus, so its effects on gene expression are relieved, basal ROS production returns, and homeostasis is maintained. Defining the specific tissues and conditions under which this nuclear cycling occurs in response to metabolic activity will be a key step to understanding the physiological role of CLK-1.

Nuclear CLK-1 suppresses the UPR^{mt}, suggesting that it acts to prevent activation of this pathway during non-stress conditions (Fig. 6). Increases in mitochondrial ROS production promote nuclear CLK-1 localization, thus maintaining ROS homeostasis but also limiting activation of the UPR^{mt}. The UPR^{mt} offers protection following the accumulation of unfolded or misfolded proteins in mitochondria, but it is not clear whether it plays a significant role in the cellular response to oxidative stress. Indeed, it has been reported that activation of the UPR^{mt} does not confer resistance to worms subjected to high levels of a mitochondrial ROS stress[11].

Our study provides the first example of a mitochondrial respiratory enzyme where two distinct forms from the same translation product are targeted to separate organelles, with the mitochondrial form participating in oxidative phosphorylation and the nuclear form acting as a sensor of metabolic activity through regulating gene expression. Dual targeting of metabolic enzymes to mitochondria and other organelles may be a common theme in cells[38] and examples of mitochondrial enzymes having nuclear roles have been reported[35,39–41]. One example is the pyruvate dehydrogenase complex (PDC) that has been shown to translocate from mitochondria to the nucleus in response to growth factor stimulation and respiratory chain inhibition. There, it facilitates acetyl-CoA synthesis and promotes histone acetylation[41]. Interestingly, in contrast to CLK-1, PDC is proposed to translocate to the nucleus from the mitochondrial matrix as an intact complex following the mitochondrial import and cleavage of the N-terminal MTS domains of the individual subunits. In worms, the transcription factor ATFS-1 also localizes to both organelles but, unlike CLK-1, translocates only to the nucleus during times of mitochondrial stress when normal proteostasis is disrupted. In the absence of stress, it is degraded following mitochondrial import[11].

It will be of interest to determine whether redirection from mitochondria to nuclei represents a paradigm for other proteins in maintaining homeostasis during mitochondrial activity or dysfunction. This study contributes to our understanding of the fundamental signalling processes that mediate the response of cells and organisms to changes in respiratory activity that occur during ageing and in disease. □

METHODS

Methods and any associated references are available in the online version of the paper.

Note: Supplementary Information is available in the online version of the paper

ACKNOWLEDGEMENTS

We thank I. Donaldson and A. Hayes of the Bioinformatics and Genomic Technologies Core Facilities at the University of Manchester for providing support with regard to ChIP–chip tiling arrays. We thank M. Howard for assistance with RP-HPLC. This work was supported by the Biotechnology and Biological Sciences Research Council (BB/J014834/1 to A.J.W. and G.B.P.) and the Wellcome Trust (093176/Z/10/Z to A.J.W. and 097820/Z/11/Z to A.J.W. and G.B.P.). Some strains were provided by the *Caenorhabditis* Genetics Center, which is funded by NIH Office of Research Infrastructure Programs (P40 OD010440). We thank A. Sharrocks, P. Shore, S. H. Yang and A. Gilmore for helpful comments on the manuscript.

AUTHOR CONTRIBUTIONS

R.M.M. conceived and designed the study, performed most of the experiments, analysed the data and wrote the paper; R.G.B. generated worm strains, imaged worms and conducted lifespan experiments; K.F. generated worm strains; T.A. and N.R. screened non-nuclear COQ7 mutants; G.B.P. conceived and designed the study; A.J.W. conceived and designed the study, analysed the data and wrote the paper.

COMPETING FINANCIAL INTERESTS

The authors declare no competing financial interests.

Published online at http://dx.doi.org/10.1038/ncb3170
Reprints and permissions information is available online at www.nature.com/reprints

1. Tait, S. W. & Green, D. R. Mitochondria and cell signalling. *J. Cell Sci.* **125,** 807–815 (2012).
2. Chandel, N. S. Mitochondria as signaling organelles. *BMC Biol.* **12,** 34 (2014).
3. Sena, L. A. & Chandel, N. S. Physiological roles of mitochondrial reactive oxygen species. *Mol. Cell* **48,** 158–167 (2012).
4. Whelan, S. P. & Zuckerbraun, B. S. Mitochondrial signaling: forwards, backwards, and in between. *Oxid. Med. Cell. Longev.* **2013,** 351613 (2013).
5. Kotiadis, V. N., Duchen, M. R. & Osellame, L. D. Mitochondrial quality control and communications with the nucleus are important in maintaining mitochondrial function and cell health. *Biochim. Biophys. Acta* **1840,** 1254–1265 (2014).
6. Yee, C., Yang, W. & Hekimi, S. The intrinsic apoptosis pathway mediates the pro-longevity response to mitochondrial ROS in *C. elegans*. *Cell* **157,** 897–909 (2014).
7. Lopez-Otin, C., Blasco, M. A., Partridge, L., Serrano, M. & Kroemer, G. The hallmarks of aging. *Cell* **153,** 1194–1217 (2013).
8. Riera, C. E. & Dillin, A. Tipping the metabolic scales towards increased longevity in mammals. *Nat. Cell Biol.* **17,** 196–203 (2015).
9. Yun, J. & Finkel, T. Mitohormesis. *Cell Metab.* **19,** 757–766 (2014).

10. Schulz, T. J. *et al.* Glucose restriction extends *Caenorhabditis elegans* life span by inducing mitochondrial respiration and increasing oxidative stress. *Cell Metab.* **6,** 280–293 (2007).
11. Nargund, A. M., Pellegrino, M. W., Fiorese, C. J., Baker, B. M. & Haynes, C. M. Mitochondrial import efficiency of ATFS-1 regulates mitochondrial UPR activation. *Science* **337,** 587–590 (2012).
12. Houtkooper, R. H. *et al.* Mitonuclear protein imbalance as a conserved longevity mechanism. *Nature* **497,** 451–457 (2013).
13. Jensen, M. B. & Jasper, H. Mitochondrial proteostasis in the control of aging and longevity. *Cell Metab.* **20,** 214–225 (2014).
14. Dillin, A. *et al.* Rates of behavior and aging specified by mitochondrial function during development. *Science* **298,** 2398–2401 (2002).
15. Marbois, B. N. & Clarke, C. F. The COQ7 gene encodes a protein in *Saccharomyces cerevisiae* necessary for ubiquinone biosynthesis. *J. Biol. Chem.* **271,** 2995–3004 (1996).
16. Jonassen, T. *et al.* Yeast Clk-1 homologue (Coq7/Cat5) is a mitochondrial protein in coenzyme Q synthesis. *J. Biol. Chem.* **273,** 3351–3357 (1998).
17. Wong, A., Boutis, P. & Hekimi, S. Mutations in the *clk-1* gene of *Caenorhabditis elegans* affect developmental and behavioral timing. *Genetics* **139,** 1247–1259 (1995).
18. Ewbank, J. J. *et al.* Structural and functional conservation of the *Caenorhabditis elegans* timing gene *clk-1*. *Science* **275,** 980–983 (1997).
19. Jonassen, T., Larsen, P. L. & Clarke, C. F. A dietary source of coenzyme Q is essential for growth of long-lived *Caenorhabditis elegans clk-1* mutants. *Proc. Natl Acad. Sci. USA* **98,** 421–426 (2001).
20. Levavasseur, F. *et al.* Ubiquinone is necessary for mouse embryonic development but is not essential for mitochondrial respiration. *J. Biol. Chem.* **276,** 46160–46164 (2001).
21. Liu, X. *et al.* Evolutionary conservation of the *clk-1*-dependent mechanism of longevity: loss of *mclk1* increases cellular fitness and lifespan in mice. *Genes Dev.* **19,** 2424–2434 (2005).
22. Felkai, S. *et al.* CLK-1 controls respiration, behavior and aging in the nematode *Caenorhabditis elegans*. *EMBO J.* **18,** 1783–1792 (1999).
23. Jiang, N., Levavasseur, F., McCright, B., Shoubridge, E. A. & Hekimi, S. Mouse CLK-1 is imported into mitochondria by an unusual process that requires a leader sequence but no membrane potential. *J. Biol. Chem.* **276,** 29218–29225 (2001).
24. Wright, G., Terada, K., Yano, M., Sergeev, I. & Mori, M. Oxidative stress inhibits the mitochondrial import of preproteins and leads to their degradation. *Exp. Cell Res.* **263,** 107–117 (2001).
25. Yang, W. & Hekimi, S. A mitochondrial superoxide signal triggers increased longevity in *Caenorhabditis elegans*. *PLoS Biol.* **8,** e1000556 (2010).
26. Van Raamsdonk, J. M. *et al.* Decreased energy metabolism extends life span in *Caenorhabditis elegans* without reducing oxidative damage. *Genetics* **185,** 559–571 (2010).
27. Matés, J. M. *et al.* Glutamine homeostasis and mitochondrial dynamics. *Int. J. Biochem. Cell Biol.* **41,** 2051–2061 (2009).
28. Suzuki, S. *et al.* Phosphate-activated glutaminase (GLS2), a p53-inducible regulator of glutamine metabolism and reactive oxygen species. *Proc. Natl Acad. Sci. USA* **107,** 7461–7466 (2010).
29. O'Keefe, L. V. *et al. Drosophila* orthologue of WWOX, the chromosomal fragile site *FRA16D* tumour suppressor gene, functions in aerobic metabolism and regulates reactive oxygen species. *Hum. Mol. Genet.* **20,** 497–509 (2011).
30. Cristina, D., Cary, M., Lunceford, A., Clarke, C. & Kenyon, C. A regulated response to impaired respiration slows behavioral rates and increases lifespan in *Caenorhabditis elegans*. *PLoS Genet.* **5,** e1000450 (2009).
31. Itoh, K., Ye, P., Matsumiya, T., Tanji, K. & Ozaki, T. Emerging functional cross-talk between the Keap1-Nrf2 system and mitochondria. *J. Clin. Biochem Nutr.* **56,** 91–97 (2015).
32. Papa, L. & Germain, D. Estrogen receptor mediates a distinct mitochondrial unfolded protein response. *J. Cell Sci.* **124,** 1396–1402 (2011).
33. Aldridge, J. E., Horibe, T. & Hoogenraad, N. J. Discovery of genes activated by the mitochondrial unfolded protein response (mtUPR) and cognate promoter elements. *PloS ONE* **2,** e874 (2007).
34. Kayser, E. B., Sedensky, M. M., Morgan, P. G. & Hoppel, C. L. Mitochondrial oxidative phosphorylation is defective in the long-lived mutant *clk-1*. *J. Biol. Chem.* **279,** 54479–54486 (2004).
35. Hall, D. A. *et al.* Regulation of gene expression by a metabolic enzyme. *Science* **306,** 482–484 (2004).
36. Lee, S. J., Hwang, A. B. & Kenyon, C. Inhibition of respiration extends *C. elegans* life span via reactive oxygen species that increase HIF-1 activity. *Curr. Biol.* **20,** 2131–2136 (2010).
37. Owusu-Ansah, E., Song, W. & Perrimon, N. Muscle mitohormesis promotes longevity via systemic repression of insulin signaling. *Cell* **155,** 699–712 (2013).
38. Yogev, O. & Pines, O. Dual targeting of mitochondrial proteins: mechanism, regulation and function. *Biochim. Biophys. Acta* **1808,** 1012–1020 (2011).
39. Yogev, O. *et al.* Fumarase: a mitochondrial metabolic enzyme and a cytosolic/nuclear component of the DNA damage response. *PLoS Biol.* **8,** e1000328 (2010).
40. Chueh, F. Y. *et al.* Nuclear localization of pyruvate dehydrogenase complex-E2 (PDC-E2), a mitochondrial enzyme, and its role in signal transducer and activator of transcription 5 (STAT5)-dependent gene transcription. *Cell. Signal.* **23,** 1170–1178 (2011).
41. Sutendra, G. *et al.* A nuclear pyruvate dehydrogenase complex is important for the generation of acetyl-CoA and histone acetylation. *Cell* **158,** 84–97 (2014).

DOI: 10.1038/ncb3170

METHODS

Plasmids and molecular cloning. pcDNA3.1-COQ7, pcDNA3.1-COQ7(37-217), pcDNA3.1-COQ7-3xMyc (C-terminal 3xMyc tag), pEGFP-N1-COQ7 (C-terminal GFP tag), pEGFP-C2-COQ7 (N-terminal GFP tag), pEGFP-C2-COQ7(11–217) (N-terminal GFP tag), pEGFP-C2-COQ7(30–217) (N-terminal GFP tag), pGEX6P1-COQ7 and pGEX6P1-COQ7(1–37) (N-terminal GST tags) were cloned by PCR amplification followed by restriction digest and ligation into the respective parent plasmid. pcDNA3.1-COQ7(R28A), pcDNA3.1-COQ7(S36A), pcDNA3.1-COQ7(R11/14/16D)-3xMyc (C-terminal 3xMyc tag), pEGFP-N1-COQ7(R21A) (C-terminal GFP tag), pEGFP-N1-COQ7(Y26F) (C-terminal GFP tag), pEGFP-N1-COQ7(R28A) (C-terminal GFP tag), pcDNA3.1(CM) (CMV minimal promoter −58 to +63), pcDNA3.1(CM)-COQ7-OLLAS (sequence encoding OLLAS tag (SGFANELGPRLMGKR) inserted between amino acids 33 and 34), pcDNA3.1(CM)-COQ7-OLLAS/FLAG (sequence encoding OLLAS tag inserted between amino acids 33 and 34 and C-terminal FLAG tag), pcDNA3.1(CM)-COQ7(R28A)-OLLAS/FLAG (sequence encoding OLLAS tag inserted between amino acids 33 and 34 and C-terminal FLAG tag), and pcDNA3.1(CM)-COQ7(R11/14/16D)-3xMyc (C-terminal 3xMyc tag) were generated with the QuikChange Lightning site-directed mutagenesis kit (Agilent Technologies). Primer sequences for cloning/mutagenesis are available on request.

siRNA. Knockdown of endogenous *COQ7* transcripts was performed using a pool of siRNAs against 5′-UTR: 5′-AGCAACCACUUCGUUGAACUU-3′ and 5′-ACUUCGUUGAACGGAACUGUU-3′; and 3′-UTR: 5′-ACCUGUUUCUCUGCAAAUGUU-3′. siRNAs were designed using the siRNA design tool from the Whitehead Institute for Biomedical Research and ordered from Eurofins Genomics.

Cell culture, transfections and stable cell lines. HeLa, COS7 and HEK293 cells were obtained from ATCC and maintained in Dulbecco's modified Eagle's medium supplemented with 5 mM glutamine, 100 units ml^{-1} penicillin/streptomycin, and 10% fetal bovine serum (Life Technologies). Plasmid DNA transfections were performed with jetPEI (Polyplus) and siRNA transfections with Lipofectamine RNAiMAX (Life Technologies). HEK293 stable cell lines were selected with 1 mg ml^{-1} G418 (Sigma) following transfection with pcDNA3.1-COQ7 or pcDNA3.1-COQ7(R28A), before monoclonal isolation and expansion. Hydrogen peroxide (Sigma), *tert*-butyl hydroperoxide (Luperox TBH70X, Sigma), and cobalt (II) chloride hexahydrate (Sigma) were diluted in water before use; HTRA2 inhibitor, UCF-101 (Calbiochem), was resuspended in DMSO.

Antibody generation and purification. COQ7 antibodies were raised in rabbits using bacterially expressed GST–COQ7 as an immunogen. Rabbits were immunized and serum was collected off-site (Genscript) and antibodies were purified against the N terminus, essentially as described previously[42]. Briefly, bacterially expressed GST or GST–COQ7(1–37) bound to GSH-Sepharose were washed twice in 0.2 M borate pH 8.6 before incubation in 20 mM dimethyl pimelimidate in 0.2 M triethanolamine pH 8.3 for 30 min to crosslink the proteins to the resin. Crosslinking was terminated by addition of 0.2 M ethanolamine pH 8.2 for 1 h before two washes in 0.1 M glycine pH 2.5 to remove non-covalently linked molecules before equilibration in TBS (15 mM Tris-HCl pH 7.4, 150 mM NaCl). Antibodies to be purified were adjusted to ×1 TBS before incubation with GSH–GST crosslinked resin for 4 h and GST-specific antibodies were removed by centrifugation. The supernatant was added to GSH–GST–COQ7(1–37) crosslinked resin, incubated for 18 h and washed. COQ7(1–37)-specific antibodies ($COQ7^{N\text{-}term2}$) were eluted with 0.1 M glycine pH 2.5 before pH adjustment to neutral with 2 M Tris. $COQ^{N\text{-}term}$ anti-COQ7(1-37)-specific antibodies were derived using the same protocol but starting with anti-COQ7 (Santa Cruz, sc-135040). For $COQ7^{FL}$ antibodies used in ChIP experiments, GST-cleared supernatants were incubated with GSH–GST–COQ7 (full length) before glycine elution.

Antibodies. The following antibodies were used for protein identification: anti-c-Jun (JUN, Santa Cruz, sc-1694, western blot (WB) 1:500); anti-CLPP (Santa Cruz, sc-134496, WB 1:500); anti-COQ7 (Proteintech, 15083-1-AP, WB 1:2,000, immunofluorescence (IF) 1:500); anti-COXIV (Pierce, MA5-15078, WB: 1:2,000); anti-FLAG (M2, Sigma, F1804, IF 1:500); anti-GLS2 (Abcam, ab113509, WB 1:500); anti-HSPA9 (Grp75/mtHsp70, Cell Signaling, 2816S, WB 1:1,000); anti-HSPD1 (HSP60, BD Transduction Laboratories, 611562, WB 1:2,000); anti-HTRA2 (OMI, Biovision, 3497-100, WB 1:1,000); anti-lamin B1 (LMNB1, Santa Cruz, sc-6216, WB 1:2,000); anti-MTCO1 (1D6E1A8, Life Technologies, 459600, WB 1:2,000); anti-Myc (4A6, Millipore, 05-742, WB 1:2,000, IF 1:500); anti-NRF2 (NFE2L2, Santa Cruz, sc-722, WB 1:500); anti-WWOX (Cell Signaling, 4045, WB 1:500); anti-OLLAS (Novus Biologicals, NBP1-06713, WB 1:500 and Genscript, A01658, IF 1:200); anti-tubulin β (TUBB, Abcam, ab6046, WB 1:5,000).

Immunofluorescence, microscopy and image analysis. Cells for microscopy were grown on coverslips, fixed in 4% paraformaldehyde (PFA, Sigma) for 10 min and then permeabilized in 0.2% Triton X-100 for 10 min. All steps were performed in ×1 PBS (phosphate buffered saline, Fisher). For immunofluorescence, cells were blocked in 3% bovine serum albumin (BSA) for 1 h, incubated in primary antibody in 3% BSA for 18 h, washed, incubated in Alexa Fluor-conjugated secondary antibody (1:1,000; Life Technologies) in 3% BSA for 1 h, and washed again. Coverslips were mounted in ProLong Gold with DAPI (Life Technologies). For MitoTracker (MitoTracker Red CMXRos; Life Technologies) staining, the dye was applied at 10 μM to media 30 min before cell fixation. For endogenous COQ7 immunofluorescence, cells were fixed in PFA for 5 min and permeabilized in methanol at 20 °C for 2 min, and then 0.2% Triton X-100 for 5 min. Images were collected on an Olympus BX51 upright microscope using a ×60 objective and captured using a Coolsnap ES camera (Photometrics) through MetaVue software (Molecular Devices). Images shown in Figs 1a,d,j and 2a,c and Supplementary Fig. 1b,c are representative of 3 independent experiments. Figure 1b is representative of the analysis in Supplementary Fig. 1a.

Western blotting. Western blotting was performed essentially as described previously[43]. Briefly, cell lysates, unless for fractionations, were prepared in Triton lysis buffer (TLB: 20 mM Tris-HCl pH 7.4, 150 mM NaCl, 25 mM β-glycerophosphate, 2 mM sodium pyrophosphate, 2 mM EDTA, 1% Triton X-100, 10% glycerol plus protease inhibitors). Samples were resolved by SDS–PAGE (10–13% gels) and transferred to Immobilon-P membranes (Millipore), which were then immunoblotted. Primary antibodies were detected with IRDye 800CW or IRDye 680LT secondary antibodies (1:5,000; LI-COR) using the Odyssey imaging system or HRP-conjugated secondary antibodies (Amersham Biosciences), followed by enhanced chemiluminescence (Pierce). Densitometry was performed using ImageJ. Blots shown in Figs 1e,i and 2e, and Supplementary Figs 1d and 2c, are representative of 3 independent experiments. Blots shown in Figs 1h and 2d are representative of the quantification shown in the same panels. Blots shown in Figs 4j and 6d are representative of 3 independent experiments, or, where indicated, the quantification shown in Supplementary Figs 3d and 4c, respectively.

Mitochondrial isolation. Mitochondrial isolation was performed essentially as described previously[44]. Briefly, cell pellets were resuspended in hypotonic buffer (10 mM Tris-HCl pH 7.4, 0.1 mM EDTA, 250 mM sucrose) and left on ice to swell for 10 min. Cells were homogenized on ice with 50 strokes of a Dounce homogenizer before centrifugation at 500*g* for 5 min to pellet the nuclear fraction. The supernatant was transferred to a new tube and centrifuged again at 10,000*g* for 20 min to pellet mitochondria.

Cell survival and proliferation assays. Cell survival was measured by MTT (3-(4,5-dimethylthiazol-2-yl)-2,5-diphenyltetrazolium bromide, Sigma) assay. MTT (5 mg ml^{-1}) was added to cells 4 h before experimental end points after which cells were washed and intracellular formazan (reduced MTT) solvated with 0.4 M HCl in 99% propanol for 1 h. The amount of formazan was assayed using a microplate reader spectrophotometer at $A_{570\,nm}$. Cell death was measured by lactose dehydrogenase presence in media, released from apoptotic or necrotic cells, using the CytoTox 96 Non-Radioactive Cytotoxicity Assay (Promega), following the manufacturer's instructions. MTT activity in the absence of detectable cell death was considered as proliferation.

Cellular ROS measurements. Intracellular ROS levels were determined by incubating cells with 10 μM 2′,7′-dichlorofluorescein diacetate (DCFDA, Life Technologies) for 30 min before cells being washed, lysed in TLB and centrifuged at 20,000*g* for 10 min. DCF fluorescence was measured in triplicate from supernatants using a microplate reader spectrophotometer at excitation 485 nm and emission 520 nm.

RNA isolation and quantitative reverse transcription PCR. RNA was isolated from cells using the RNeasy system (Qiagen) following the manufacturer's instructions. Contaminating DNA was removed using the DNA-free Kit (Life Technologies). Quantitative reverse transcription PCR analysis was performed for both HEK293 cells and worm samples using the Power SYBR green RNA-to-CT 1-Step Kit (Life Technologies) following the manufacturer's instructions, with 10 μl reactions. Each experimental repeat was run in triplicate. Primer sequences can be found in Supplementary Table 3. References for primer sequences are available on request. Reference genes for quantification: human, *RPL19*; *C. elegans*, *act-1* and *tba-1*. Changes in gene expression were quantified using the $\Delta\Delta$Ct method[45], normalizing for each gene to the reference gene for the same sample and then to one control sample, as indicated in the figure legends. The heat map in Fig. 6c was generated using Multi Experiment Viewer software and represents the mean values of four independent experimental repeats (Supplementary Fig. 4b).

Quinone extraction and reverse-phase high-performance liquid chromatography. Quinone extraction and determination was performed essentially as described previously[46]. Briefly, cell or worms pellets that had been frozen and thawed three times were resuspended in lysis buffer (15 mM Tris-HCl pH 7.4, 150 mM NaCl, 0.1% SDS) and vortexed. Quinones were extracted by vortexing resuspended pellets in ethanol/hexane (2/5, v/v) for 10 min followed by centrifugation at 20,000*g* for 5 min and the top hexane supernatant layer was removed. This was repeated three times and the supernatants were combined. Hexane was removed by drying in a SpeedVac Concentrator and the residue was resuspended in ethanol. Resuspended quinones were applied to a reverse-phase column (Jupiter 4 µm Proteo 90 Å, C-12, 250 × 4.6 mm, Phenomenex) and eluted in isocratic conditions (1 ml min^{-1}, diisopropyl ether/methanol (1/4, v/v)) by high-performance liquid chromatography (Ettan LC, GE Healthcare). Eluted quinones were compared using their retention times and ultraviolet spectrophotometry ($A_{275\,nm}$). Ubiquinone-10 (Coenzyme Q10, Sigma) and ubiquinone-9 (Sigma) were used as standards for human and *C. elegans* endogenous ubiquinone, respectively. Clioquinol (Vetranal, Sigma) was used to inhibit COQ7 activity[47] leading to accumulation of its substrate demethoxyubiquinone-10. Chromatograms in Figs 2f and 3c and Supplementary Fig. 2e are representative of 3 independent experiments.

Chromatin fractionation. Isolation of chromatin/DNA-associated protein complexes from cells was performed essentially as described previously[48]. Briefly, cells were washed then scraped in CSK buffer (10 mM PIPES pH 6.8, 300 mM sucrose, 100 mM NaCl, 3 mM magnesium chloride, 1 mM EGTA, 0.5% Triton X-100 plus protease inhibitors) and left at 4 °C for 5 min before centrifugation at 5,000*g* for 3 min. The supernatant was removed as the Triton-soluble fraction. The pellet was resuspended in CSK buffer containing 30 U DNase I (New England Biolabs) and incubated at 37 °C for 20 min followed by precipitation of chromatin by addition of 0.25 M ammonium sulphate and incubation at 4 °C for 5 min. Samples were then centrifuged at 5,000*g* for 3 min and the supernatant was taken as the DNase-soluble fraction.

Chromatin immunoprecipitation. Chromatin immunoprecipitations (ChIPs) for qPCR analysis of promoter regions or promoter microarray were carried out essentially as described previously[49]. Cells were washed then crosslinked in 0.85% formaldehyde for 10 min at 20 °C before quenching with a final concentration of 0.125 M glycine for 5 min. Cells were then washed and lysed in FA buffer (50 mM Tris pH 8, 150 mM NaCl, 1 mM EDTA, 1% Triton X-100, 0.1% sodium deoxycholate, 0.1% SDS, protease inhibitors) for 10 min at 4 °C followed by sonication using a 4 °C water bath sonicator (Bioruptor Sonicator, Diagenode) set to medium power with cycles of 30 s on 30 s off for 5 min or until an average DNA fragment length of 0.3–0.7 kb was obtained. Samples were centrifuged at 21,000*g* for 10 min before addition of ABRI buffer (50 mM Tris pH 8,150 mM NaCl, 1 mM EDTA, 0.5% NP-40, 0.5% sodium deoxycholate, protease inhibitors) 3:1 to supernatants. A 1/20 fraction of each sample was taken as input and the rest was used for immunoprecipitations. Two micrograms of each antibody ($COQ7^{FL}$ or rabbit IgG control, Santa Cruz, sc-2027) was added before rotation for 18 h at 4 °C and addition of 15 µl pre-washed protein A Dynabeads (Life Technologies) for a further 1 h. ChIPed complexes were washed once in ABRI buffer, twice in WB1 buffer (20 mM Tris pH 8, 2 mM EDTA, 150 mM NaCl, 1% Triton X-100), twice in WB2 buffer (20 mM Tris pH 8, 2 mM EDTA, 250 mM LiCl, 0.5% NP-40, 0.5% sodium deoxycholate), and once in TE buffer (25 mM Tris, 1 mM EDTA) before elution in 1% SDS and 0.1 M $NaCHO_3$ with rotation/shaking at 30 °C for 30 min. Eluted complexes and inputs were then adjusted to 150 mM NaCl and crosslinks were reversed by incubation at 65 °C for 18 h. Samples were then treated with proteinase K (Sigma) for 2 h at 50 °C. ChIPed and input DNA was then phenol/chloroform/IAA (Sigma) purified and washed before final solvation in TE buffer. For qPCR analysis of promoter enrichment, primers against regions of interest (Supplementary Table 3) were used to amplify DNA in both ChIPs and inputs and antibody enrichment calculated as a percentage of input using the following formulae: 2^X = input dilution factor, total input Ct value = input Ct–X, sample percentage of input = $2^{(\text{total input Ct}-\text{sample Ct})} \times 100$. For promoter microarray analysis, DNA samples for IgG control or COQ7 ChIPs were amplified using random-primer PCR amplification. DNA was subjected to two rounds of PCR. Initial reactions of 40 ng DNA, ×1 Sequenase buffer (US Biochemical) and 5 µM of the degenerate primer 5′-GTTTCCCAGTCACGATCNNNNNNNNN-3′ were subjected to two cycles of primer extension: 98 °C for 5 min, 8 °C for 4 min, slow ramped (10%) from 8 to 37 °C before a further 8 min at 37 °C. During the first 8 °C hold the reaction mixture was adjusted to 0.25 mM dNTPs, 3 mM dithiothreitol and 0.05 mg ml^{-1} BSA; during the second 8 °C hold 1.5 U μl^{-1} Sequenase (US Biochemical) was added. DNA was purified with a PCR Clean-up Kit (Qiagen) and all eluted DNA was then subjected to a second round of PCR with 1 U μl^{-1} Biotaq polymerase (Gentaur), 0.25 mM dNTPs, ×1 Biotaq buffer and 1 µM of the amplification primer 5′-GTTTCCCAGTCACGATC-3′ denatured at 97 °C for 3 min before 25 cycles of: 97 °C for 30 s, 40 °C for 10 s, 50 °C for 30 s and 72 °C for 90 s; followed by a final extension of 72 °C for 5 min. Amplified DNA was again purified as before and 10 µg of each sample was sent for processing at the on-site genomic technologies facility using Affymetrix GeneChip Human Promoter 1.0R Arrays. Enriched probe sets were analysed for two repeats of the experiment and regions significantly enriched in COQ7 ChIPs compared with IgG control are listed in Supplementary Table 2.

***C. elegans* strains.** *C. elegans* were cultured at 20 °C on nematode growth medium (NGM) agar plates seeded with OP50 strain *Escherichia coli*[50]. The following strains were obtained from the *Caenorhabditis* Genetics Center: SJ4100 zcIs13 [*hsp-6::gfp*], EG6699 ttTi5605; *unc-119* (ed3); oxEx1578, and stIs10116 [*phis-72::his-24::mcherry::let-858 3′ UTR*]. Other strains used were wild-type Bristol N2 and MQ130 *clk-1* (*qm30*) (ref. 17). Transgenic strains made in this study were OL0092 ukSi1[*pclk-1::clk-1::gfp, cb-unc-119*(+)], OL0119 ukSi2[*pclk-1::clk-1 ΔMTS* (*13-187*)*::gfp, cb-unc-119*(+)], OL0100 ukSi1[*pclk-1::clk-1::gfp, cb-unc-119*(+)]; *clk-1* (*qm30*), OL0177 ukSi1[*pclk-1::clk-1::gfp, cb-unc-119*(+)]; stIs10116[*phis-72::his-24::mcherry::let-858 3′ UTR*], OL0120 ukSi2[*pclk-1::clk-1 ΔMTS* (*13-187*)*::gfp, cb-unc-119*(+)]; *clk-1* (*qm30*), OL0121 *clk-1* (*qm30*); *hsp-6::gfp* and OL0123 ukSi2[*pclk-1::clk-1 ΔMTS* (*13-187*)*::gfp, cb-unc-119*(+)]; *clk-1* (*qm30*); *hsp-6::gfp*.

Generation of *C. elegans* transgenic strains. Transgenic strains OL0092 and OL0119 were generated using MosI-mediated single copy insertion (MosSCI) as described previously[51]. Briefly, a plasmid containing *pclk-1::clk-1::gfp* was generated using Gateway techniques (Invitrogen). pDONR clones were generated for the *clk-1* promoter and open reading frame using Gateway and gene-specific primers. The vector pJA256 (ref. 52) was used as the pDONR clone for GFP. The final destination vector used was pCFJ150, which contains an *unc-119* rescue fragment. *pclk-1::clk-1 ΔMTS (13-187)::gfp* was generated by mutagenesis of the *pclk-1::clk-1::gfp* plasmid. Primer sequences are available on request. MosSCI was performed using the direct injection protocol. *unc-119* animals were injected with an injection mix consisting of: pCFJ150 containing *pclk-1::clk-1::gfp* or *pclk-1::clk-1 ΔMTS (13-187)::gfp* (50 ng μl^{-1}), pCFJ601 (50 ng μl^{-1}), pMA122 (10 ng μl^{-1}), pGH8 (10 ng μl^{-1}), pCFJ90 (2.5 ng μl^{-1}) and pCFJ104 (5 ng μl^{-1}). Selection was based on heat shock survival, wild-type movement, no expression of mCherry markers and GFP expression. Insertion of the transgene was confirmed by sequencing.

Worm imaging. MitoTracker staining was performed as follows. Approximately 2–3-day-old adult worms were washed off NGM agar plates using M9 buffer. Worms were washed twice in M9 buffer, and then once in MR buffer (10 µM MitoTracker Red CMXRos (Invitrogen) in M9 buffer), before being incubated in MR buffer for 2 h on a rotating mixer at room temperature in the dark. The worms were then pelleted before being washed once with M9 buffer and being allowed to recover on a standard NGM agar plate for 1 h at 20 °C. They were then mounted on agarose pads and imaged at ×100 magnification on a Leica DM5000B fluorescence microscope and images were captured by a Leica DFC340FX camera. Cells in the tail region were imaged. For NAC experiments, synchronized *clk-1::gfp; his-24::mcherry* worms were grown on untreated NGM agar plates or plates containing 10 mM NAC. Adult worms were imaged as described and the proportion of nuclear CLK-1–GFP was determined by co-localization with the HIS-24–mCherry nuclear marker. For *hsp-6::gfp* reporter assays, between 40 and 60 young adult worms were mounted on agarose pads as described and imaged at ×5 magnification. Fluorescence intensity was quantified using ImageJ. Images shown in Figs 1c and 3b are representative of >6 independent experiments.

Measurement of worm ROS levels. ROS were measured using dihydroethidium (DHE). Briefly, synchronized adult worms were washed 3 times in PBS and then incubated in 3 µM DHE for 30 min. Following incubation worms were washed in PBS and then mounted on agarose pads and imaged at ×63 magnification. The fluorescence intensity in the head of the worm was quantified using ImageJ.

Paraquat sensitivity assay. Synchronized adult worms were treated with 40 mM Paraquat, dissolved in M9 buffer, for 6 h in a 96-well plate. Approximately 25 worms were plated in each well, with each strain measured in triplicate. Survival was measured every 2 h with worms being scored as dead if they failed to respond to gentle tapping of the plate.

Lifespan assays. Lifespan assays were performed as described previously[53]. Briefly, 100 synchronized L1 stage worms were plated onto standard NGM agar plates seeded with OP50 bacteria. On reaching adulthood worms were transferred daily to fresh plates until egg laying ceased. Worms were scored daily, being judged as dead when they failed to respond to gentle prodding from a worm pick. Any worms that crawled off the plates during the assay were censored. Presented lifespan plots are representative of lifespan from the L1 larval stage from 3

DOI: 10.1038/ncb3170

independent experiments. The full analysis is presented in Supplementary Table 1. The experiments were not randomized and the investigators were not blinded to allocation during experiments and outcome assessment. No statistical methods were used to predetermine sample size.

Development assays. Gravid adult worms were bleached and the embryos plated on NGM agar plates without food overnight. Synchronized L1 worms were transferred to spotted NGM plates and larval stage was determined every 24 h until all of the worms reached adulthood. Approximately 50 worms per time point for each genotype were mounted on agarose pads and scored then discarded.

Worm RNA extraction. Synchronized day 1 adult worms were pelleted and vortexed in 250 µl Trizol (Life Technologies) for 2 min and left for 30 min to dissolve. Fifty microlitres of chloroform was added and tubes were vortexed for 2 min before centrifugation at 20,000*g* for 5 min. The supernatant was removed to a new tube and 125 µl of propanol was added for 30 min before centrifugation at 20,000*g* for 5 min. The supernatant was discarded and the pellet was dissolved in RNase-free water. Contaminating DNA was removed using the DNA-free Kit (Life Technologies).

Statistical analysis. Values are expressed as mean; error bars represent the standard error of the mean. Data were analysed, unless otherwise stated, using unpaired Student's *t*-test and confidence is given by the *P* values indicated in the figure legends. For analysis of the proportion of cells with nuclear staining (Supplementary Fig. 1a) a *z*-test was used. For lifespan assays, survival time was estimated with the Kaplan–Meier method and the log-rank method was applied to compare survival curves.

Accession numbers. The ArrayExpress accession code for the ChIP array is E-MTAB-3433.

42. Bar-Peled, M. & Raikhel, N. V. A method for isolation and purification of specific antibodies to a protein fused to the GST. *Anal. Biochem.* **241,** 140–142 (1996).
43. Whitmarsh, A. J. & Davis, R. J. Analyzing JNK and p38 mitogen-activated protein kinase activity. *Methods Enzymol.* **332,** 319–336 (2001).
44. Frezza, C., Cipolat, S. & Scorrano, L. Organelle isolation: functional mitochondria from mouse liver, muscle and cultured fibroblasts. *Nat. Protoc.* **2,** 287–295 (2007).
45. Livak, K. J. & Schmittgen, T. D. Analysis of relative gene expression data using real-time quantitative PCR and the 2(-$\Delta\Delta$ C(T)) method. *Methods* **25,** 402–408 (2001).
46. Miyadera, H. *et al.* Quinones in long-lived clk-1 mutants of *Caenorhabditis elegans*. *FEBS Lett.* **512,** 33–37 (2002).
47. Wang, Y. *et al.* The anti-neurodegeneration drug clioquinol inhibits the aging-associated protein CLK-1. *J. Biol. Chem.* **284,** 314–323 (2009).
48. Mirzoeva, O. K. & Petrini, J. H. DNA replication-dependent nuclear dynamics of the Mre11 complex. *Mol. Cancer Res.* **1,** 207–218 (2003).
49. Aparicio, O. *et al.* Chromatin immunoprecipitation for determining the association of proteins with specific genomic sequences *in vivo*. *Curr. Protoc. Mol. Biol.* http://dx.doi.org/10.1002/0471143030.cb1707s23 (2005).
50. Brenner, S. The genetics of *Caenorhabditis elegans*. *Genetics* **77,** 71–94 (1974).
51. Frokjaer-Jensen, C. *et al.* Single-copy insertion of transgenes in *Caenorhabditis elegans*. *Nat. Genet.* **40,** 1375–1383 (2008).
52. Zeiser, E., Frokjaer-Jensen, C., Jorgensen, E. & Ahringer, J. MosSCI and gateway compatible plasmid toolkit for constitutive and inducible expression of transgenes in the *C. elegans* germline. *PloS ONE* **6,** e20082 (2011).
53. Lakowski, B. & Hekimi, S. Determination of life-span in *Caenorhabditis elegans* by four clock genes. *Science* **272,** 1010–1013 (1996).

DOI: 10.1038/ncb3170

nature cell biology

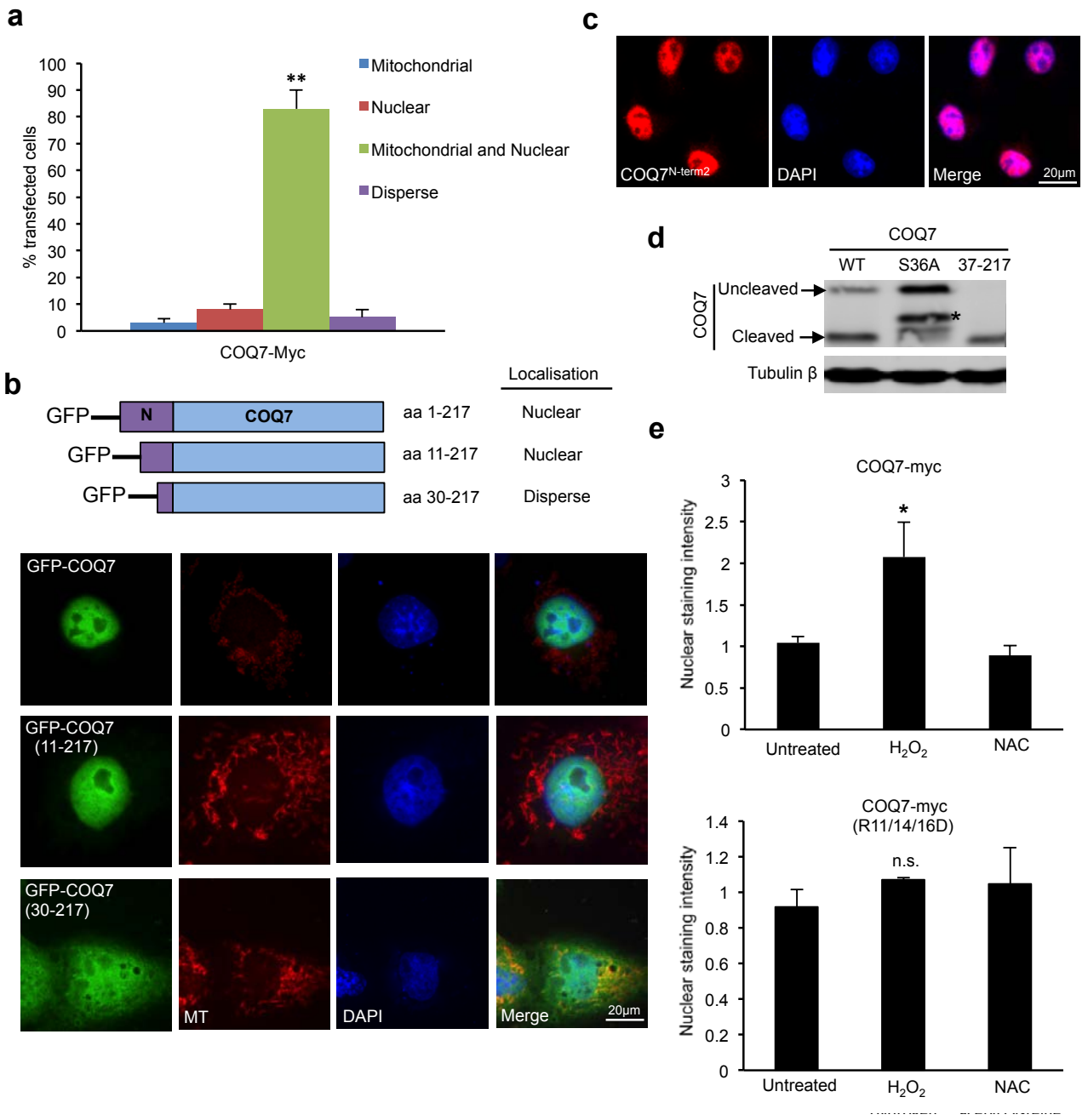

Supplementary Figure 1 A distinct pool of COQ7 localises to nuclei. **(a)** HeLa cells expressing COQ7-Myc were scored for mitochondrial, nuclear, mitochondrial and nuclear, or disperse COQ7 immunostaining (40 cells assessed in each of n=3 independent experiments; error bars, s.e.m. $^{**}P < 0.005$ compared to other localisations). Representative image of cells is shown in Fig. 1b. **(b)** The region of COQ7 required for specific nuclear localisation resides between amino acids 11 and 29. GFP fluorescence of COS7 cells expressing GFP-COQ7 and the deletion mutants GFP-COQ7(11-217), lacking amino acids 1-10, and GFP-COQ7(30-217), lacking amino acids 1-29. Orientating the GFP tag on the N-terminus of COQ7 abolished mitochondrial localisation and promoted nuclear localisation, probably due to disruption of the interaction between the N-terminal MTS and the mitochondrial import machinery. Mitochondria are stained with MitoTracker (MT) and nuclei with DAPI. Schematic depicts the GFP-COQ7 deletion mutants used and summarises their localisation. **(c)** Endogenous uncleaved COQ7 is nuclear. HeLa cells immunostained with a second antibody specific to the N-terminus of COQ7 ($COQ7^{N\text{-}term2}$). Nuclei are stained with DAPI. **(d)** Immunoblot demonstrating that uncleaved wild type COQ7 (WT) migrates at the same position as COQ7 S36A (containing a point mutation in the predicted mitochondrial processing peptidase cleavage site) and that cleaved COQ7 migrates at the same position as COQ7(37-217) that lacks the N-terminal region cleaved by MPP. * denotes partial cleavage of COQ7 S36A at a site upstream of the predicted MPP site. **(e)** The intensity of nuclear anti-Myc immunostaining in HeLa cells expressing COQ7-Myc or COQ7-R11/14/16D-Myc was quantified. Cells were treated with H_2O_2 (150 μM, 4 h) or NAC (10 mM, 6 h). 50 cells assessed in each of n=3 independent experiments; error bars, s.e.m. n.s., no significant difference; $^{*}P < 0.05$ relative to untreated.

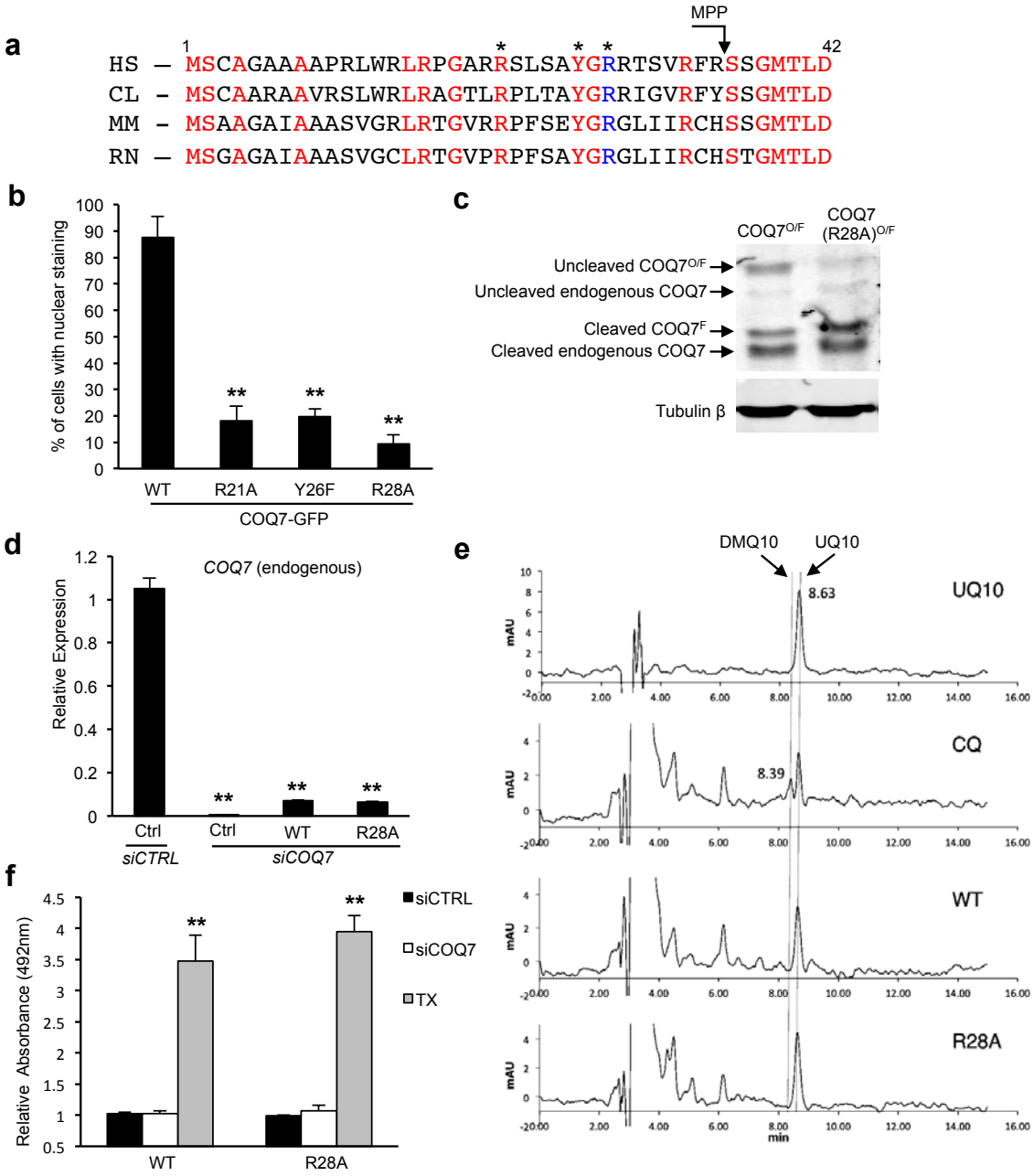

Supplementary Figure 2 Identifying a non-nuclear mutant of COQ7. **(a)** Alignment of mammalian COQ7 N-terminal protein sequences (amino acids 1 to 42) using Clone Manager (Sci-Ed Software); HS, *Homo sapiens*; CL, *Canis lupus familiaris*; MM, *Mus musculus*; RN, *Rattus norvegicus*. Conserved residues are in red and R28 is in blue. MPP marks the predicted mitochondrial processing peptidase cleavage site. Residues mutated and assessed in the fluorescence studies in panel b are denoted with asterisks. **(b)** Point mutations in the COQ7 N-terminus cause reduced nuclear localisation. GFP fluorescence in COS7 cells expressing COQ7 fused at the C-terminus to GFP and harboring the point mutations R21A, Y26F and R28A were analysed. Quantification of the percent of cells displaying nuclear staining is shown (100 cells assessed in each of n=3 independent experiments; error bars, s.e.m. $^{**}P < 0.005$). The most severe loss of nuclear staining was observed with the R28A mutation. **(c)** COQ7 (R28A) mutant displays reduced levels of the uncleaved form. Lysates from HEK293 cells expressing OLLAS and FLAG tagged COQ7 ($COQ7^{O/F}$) or COQ7(R28A)$^{O/F}$ (Fig. 2b) were immunoblotted with anti-COQ7 antibody. **(d)** Parent HEK293 cells (Ctrl) or cells stably expressing untagged (WT) or non-nuclear COQ7 (R28A) were transfected with *siCTRL* or *siCOQ7* that specifically targets endogenous *COQ7* mRNA. Transcript levels of endogenous *COQ7* mRNA (5'UTR amplicon) were analysed (mean values from 3 reactions per condition in n=4 independent experiments; error bars, s.e.m. $^{**}P < 0.005$). **(e)** Reverse phase HPLC chromatograms of quinones. Purified ubiquinone-10 (UQ10) was used as a standard. Levels of UQ10 and demethoxyubiquinone-10 (DMQ10) were measured in HEK293 cells treated with the COQ7 inhibitor clioquinol (CQ; 10 μM, 24 h), or from WT or R28A expressing HEK293 cells. CQ caused the appearance of DMQ10. UQ10 peak at 8.63 mins, DMQ10 peak at 8.39 mins. **(f)** Levels of lactate dehydrogenase (LDH) in media from cultured WT and R28A cells are similar, indicating that cell survival under basal conditions is not changed (mean values from 4 wells of cells per condition in n=3 independent experiments; error bars, s.e.m. $^{**}P < 0.005$). Treatment with 0.1% (v/v) Triton X-100 (TX) for 30 minutes was used as a positive control.

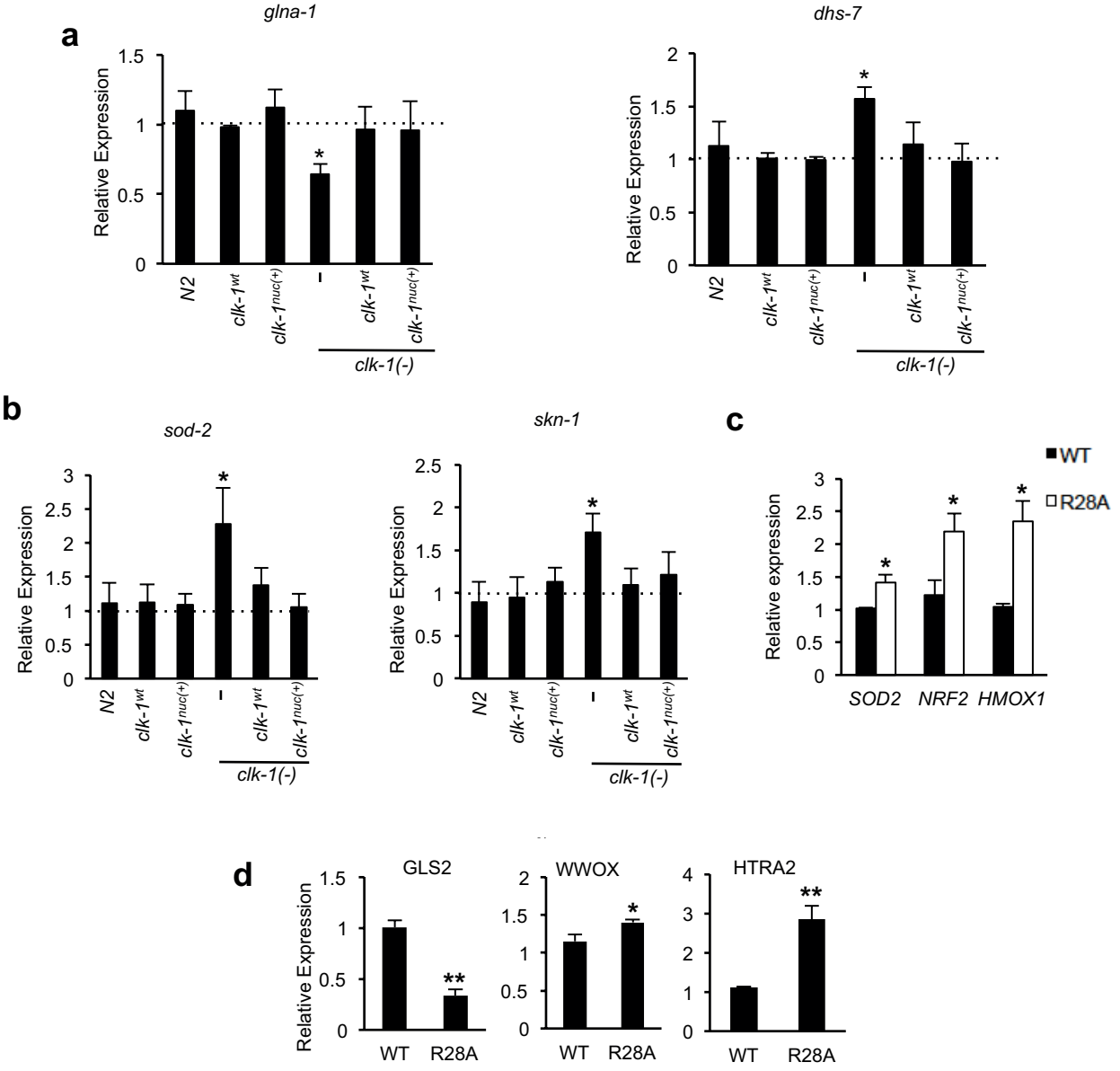

Supplementary Figure 3 Nuclear CLK-1 and COQ7 regulate ROS metabolic gene expression. **(a)** Nuclear CLK-1 regulates the expression of genes involved in ROS metabolism. qPCR analysis of transcripts from ROS-sensitive retrograde genes (mean values from 3 reactions per condition in n=3 independent experiments; error bars, s.e.m. $*P<0.05$ for *clk-1(-)* compared to other strains). **(b)** CLK-$1^{nuc(+)}$ rescues the increased transcript levels of genes known to be responsive to ROS (*sod-2* and *skn-1*) in *clk-1* null worms (mean values from 3 reactions per condition in n=3 independent experiments; error bars, s.e.m. $*P<0.05$ for *clk-1(-)* compared to other strains). **(c)** Human homologues of these genes, *SOD2* and *NRF2*, and the NRF2 target gene *HMOX1* are increased in cells that have lost nuclear COQ7 (R28A) (mean values from 3 reactions per condition for n=4 independent experiments; error bars, s.e.m. $*P < 0.05$). **(d)** Quantification of immunoblots for GLS2, WWOX and HTRA2 proteins (mean values from n=3 independent experiments; error bars, s.e.m. $*P < 0.05$, $**P < 0.005$). Representative blots are shown in Fig. 4i.

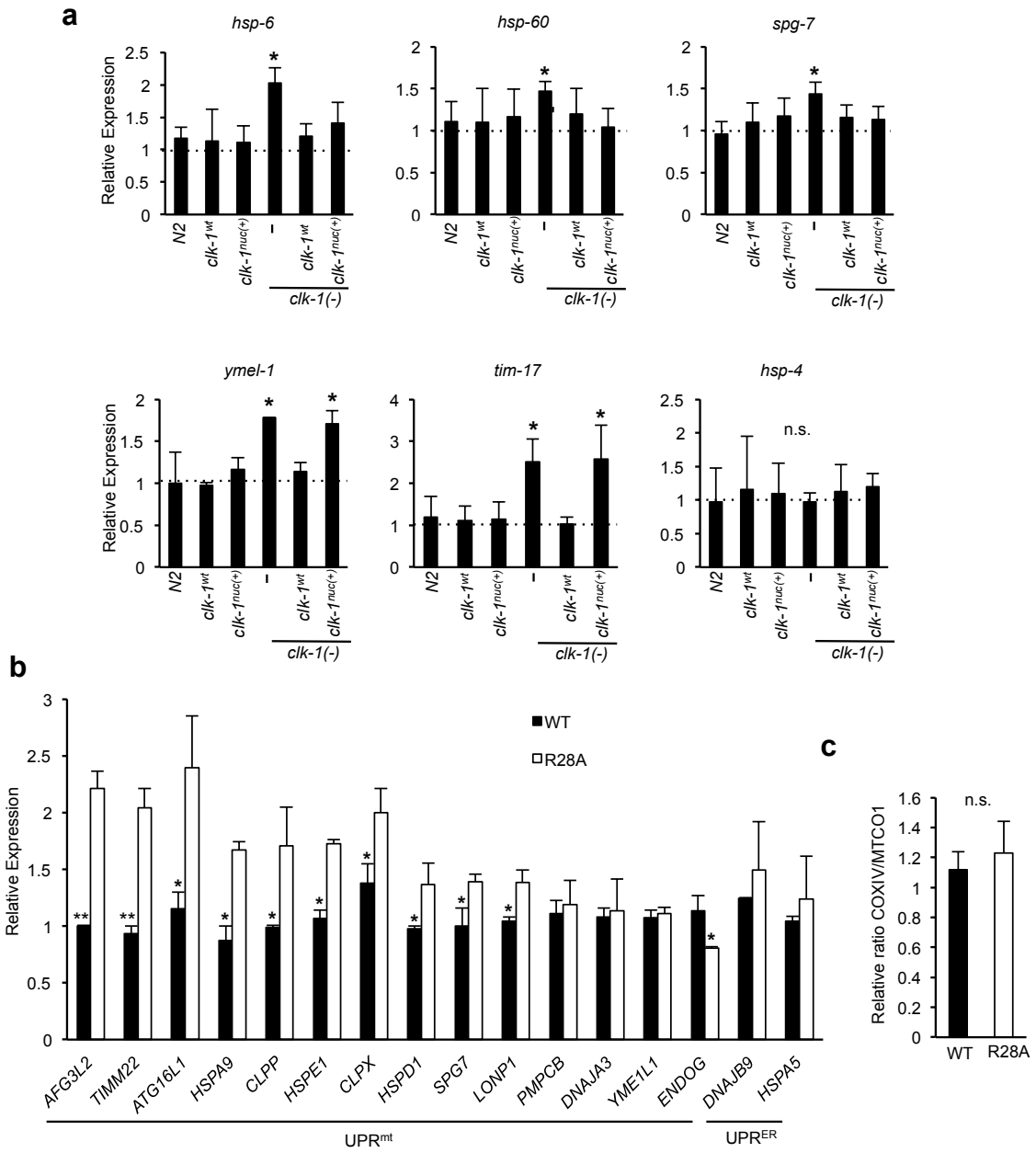

Supplementary Figure 4 Nuclear CLK-1 and COQ7 suppresses the expression of UPR^{mt} genes. **(a)** qPCR analysis of UPR^{mt} genes in CLK-1 transgenic worm strains relative to *N2* (mean values from 3 reactions per condition in n=3 independent experiments; error bars, s.e.m. n.s., no significant difference; $*P<0.05$). The increase in expression of *hsp-6*, *hsp-60* and *spg-7* in *clk-1(-)* worms was abrogated by expression of either CLK-1^{wt} or CLK-1$^{nuc(+)}$. mRNA levels of the endoplasmic reticulum UPR (UPR^{ER})-regulated gene *hsp-4* were not changed in any of the worm strains. **(b)** qPCR of analysis of transcripts of UPR^{mt} genes and UPR^{ER} genes in WT and R28A expressing HEK293 cells (mean values from 3 reactions per condition in n=4 independent experiments; error bars, s.e.m. $*P<0.05$. $**P<0.005$). Heatmap of this data is shown in Fig. 6c. **(c)** The ratio of COXIV to MTCO1 protein levels in WT and R28A expressing cells quantified from n=3 independent immunoblots (error bars, s.e.m. n.s., no significant difference). See Fig. 6d for representative immunoblot.

Figure 1i

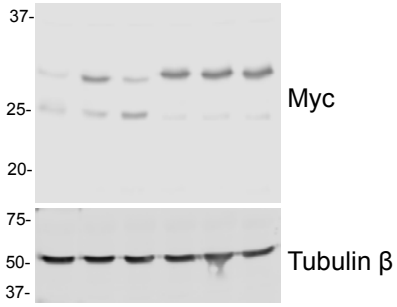

Figure 2d

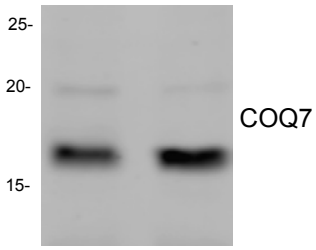

Figure 2e

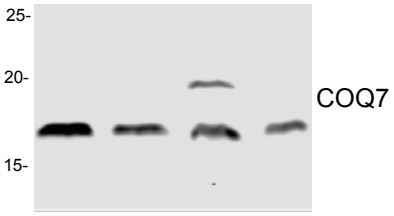

Figure 4i

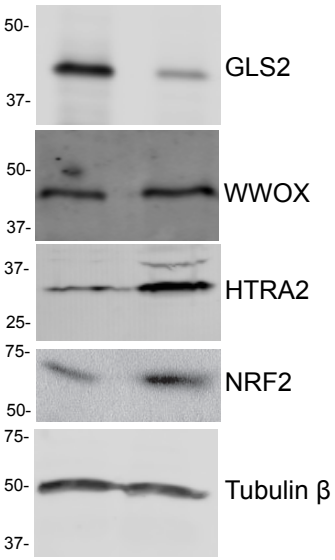

Figure 6d

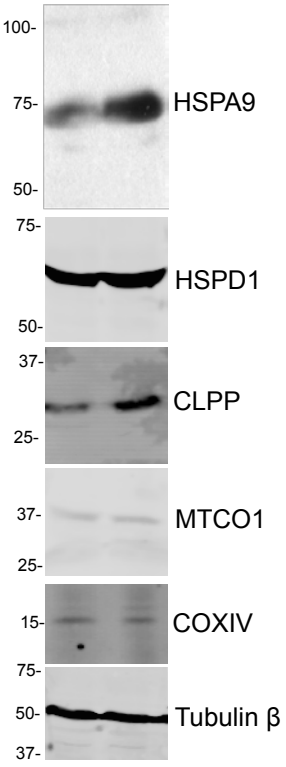

Figure 7a

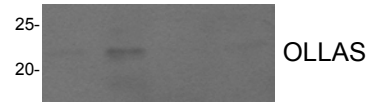

Supplementary Figure 5 Uncropped scans of western blots.

Supplementary Table Legends

Supplementary Table 1: Complete lifespan analysis of *C. elegans* strains.
CLK-1$^{nuc(+)}$ expression partially rescues the increased lifespan observed in *clk-1*(-) worms while CLK-1^{wt} completely rescues the longevity phenotype. The presented lifespan data includes the mean, maximum and 90th percentile lifespan with statistical analysis for each worm strain from 3 independent experimental repeats.

Supplementary Table 2: COQ7 chromatin-binding sites. Anti-COQ7 chromatin immunoprecipitation was performed on HEK293T cells and samples analysed by human promoter microarray as described in Methods. COQ7-specific binding sites, compared to IgG control, with fold change >2 are presented here, with nearest gene transcriptional start site (TSS) annotated (*P* values and false discovery rate (FDR) from two experimental repeats). The ArrayExpress accession code for the ChIP array is E-MTAB-3433.

Supplementary Table 3: Primer sequences for qPCR experiments.